

AD-A112 911

PHYSICS INTERNATIONAL CO SAN LEANDRO CA  
ASYMMETRIC COLLAPSE OF LOS PIPE.(U)  
MAY 80 E T MOORE, R FUNSTON

F/6 18/3

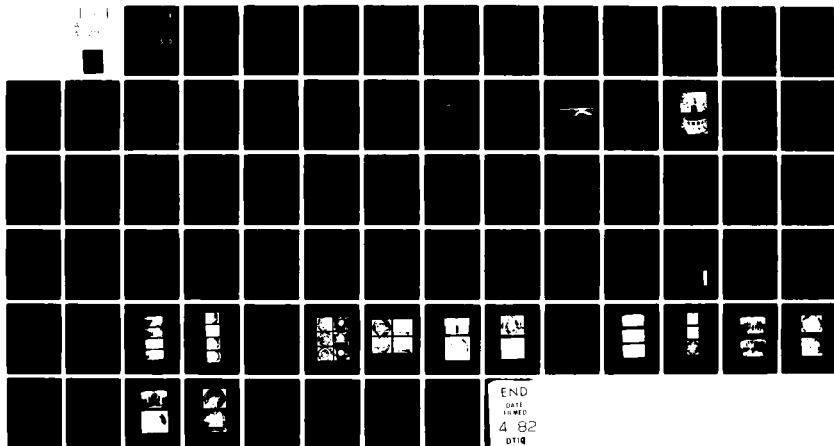
UNCLASSIFIED

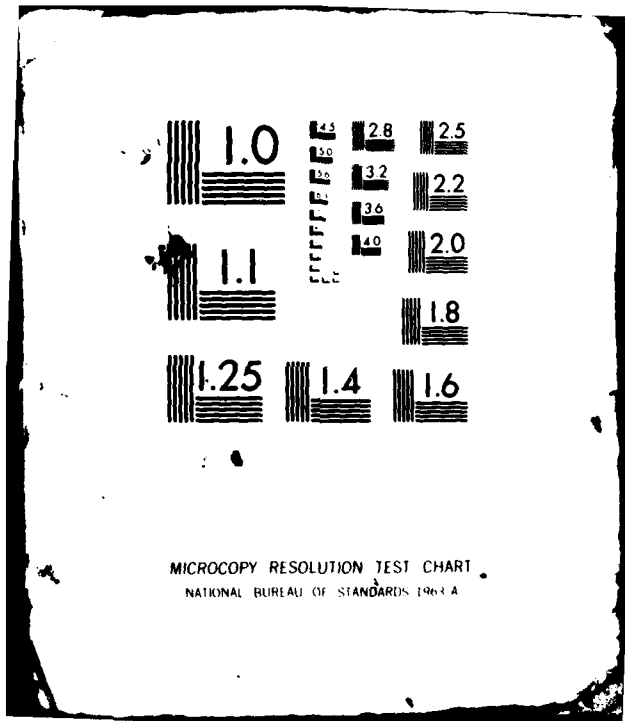
PIFR-1034-F

S81-AD-E300 953

DNA001-77-C-0155

NL



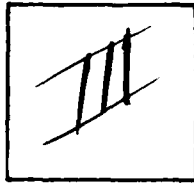


MICROCOPY RESOLUTION TEST CHART  
NATIONAL BUREAU OF STANDARDS 1963-A

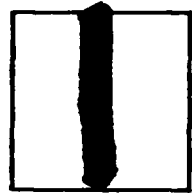
PHOTOGRAPH THIS SHEET

ADA 112911

DTIC ACCESSION NUMBER



LEVEL



INVENTORY

DOCUMENT IDENTIFICATION

Contract DNA001-77-C-0155

Final Rept.  
26 May 80  
Rept. No. PIFR-1034  
DNA-5322F

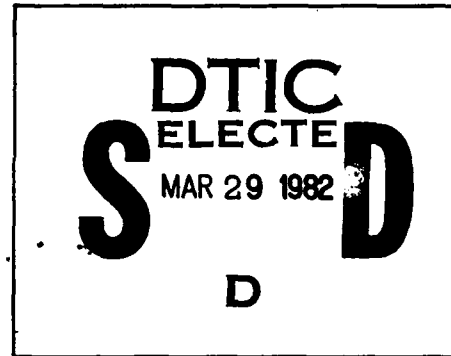
DISTRIBUTION STATEMENT A

Approved for public release;  
Distribution Unlimited

DISTRIBUTION STATEMENT

ACCESSION FOR	
NTIS	GRA&I <input checked="" type="checkbox"/>
DTIC	TAB <input type="checkbox"/>
UNANNOUNCED	<input type="checkbox"/>
JUSTIFICATION	
BY	
DISTRIBUTION /	
AVAILABILITY CODES	
DIST	AVAIL AND/OR SPECIAL
A	

DISTRIBUTION STAMP



DATE ACCESSIONED



82 03 25 002

DATE RECEIVED IN DTIC

PHOTOGRAPH THIS SHEET AND RETURN TO DTIC-DDA-2

DNA 5322F

# ASYMMETRIC COLLAPSE OF LOS PIPE

E. T. Moore, Jr.

Ron Funston

Physics International Company

2700 Merced Street

San Leandro, California 94577

26 May 1980

Final Report for Period 16 July 1979-1 September 1979

CONTRACT No. DNA 001-77-C-0155

APPROVED FOR PUBLIC RELEASE;  
DISTRIBUTION UNLIMITED.

THIS WORK SPONSORED BY THE DEFENSE NUCLEAR AGENCY  
UNDER RDT&E RMSS CODE B345079462 J24AAXYX98363 H2590D.

Prepared for

Director

DEFENSE NUCLEAR AGENCY

Washington, D. C. 20305

AD A112911

Destroy this report when it is no longer needed. Do not return to sender.

PLEASE NOTIFY THE DEFENSE NUCLEAR AGENCY,  
ATTN: STTI, WASHINGTON, D.C. 20305, IF  
YOUR ADDRESS IS INCORRECT, IF YOU WISH TO  
BE DELETED FROM THE DISTRIBUTION LIST, OR  
IF THE ADDRESSEE IS NO LONGER EMPLOYED BY  
YOUR ORGANIZATION.



UNCLASSIFIED

SECURITY CLASSIFICATION OF THIS PAGE (When Data Entered)

REPORT DOCUMENTATION PAGE		READ INSTRUCTIONS BEFORE COMPLETING FORM
1. REPORT NUMBER DNA 5322F	2. GOVT ACCESSION NO.	3. RECIPIENT'S CATALOG NUMBER
4. TITLE (and Subtitle)  ASYMMETRIC COLLAPSE OF LOS PIPE		5. TYPE OF REPORT & PERIOD COVERED Final Report for Period 16 Jul 79—1 Sep 79
		6. PERFORMING ORG. REPORT NUMBER PIFR-1034
7. AUTHOR(s)  E.T. Moore, Jr. Ron Funston		8. CONTRACT OR GRANT NUMBER(s) DNA 001-77-C-0155
9. PERFORMING ORGANIZATION NAME AND ADDRESS Physics International Company 2700 Merced Street San Leandro, California 94577		10. PROGRAM ELEMENT, PROJECT, TASK AREA & WORK UNIT NUMBERS  Subtask J24AAXYX983-63
11. CONTROLLING OFFICE NAME AND ADDRESS Director Defense Nuclear Agency Washington, D.C. 20305		12. REPORT DATE 26 May 80
		13. NUMBER OF PAGES 78
14. MONITORING AGENCY NAME & ADDRESS (if different from Controlling Office)		15. SECURITY CLASS. (of this report)  UNCLASSIFIED
		15a. DECLASSIFICATION/DOWNGRADING SCHEDULE N/A
16. DISTRIBUTION STATEMENT (of this Report)  Approved for public release; distribution unlimited.		
17. DISTRIBUTION STATEMENT (of the abstract entered in Block 20, if different from Report)		
18. SUPPLEMENTARY NOTES  This work sponsored by the Defense Nuclear Agency under RDT&E RMSS Code B345079462 J24AAXYX98363 H2590D.		
19. KEY WORDS (Continue on reverse side if necessary and identify by block number) Underground nuclear testing      Jetting Nuclear                                      Line-of-sight Explosives                                  Stem g Containment		
20. ABSTRACT (Continue on reverse side if necessary and identify by block number)  A single laboratory experiment was performed to further evaluate the feasibility of using asymmetries to suppress jetting in line-of-sight (LOS) pipes that are collapsed by the ground shock from an underground nuclear test. Underground conditions were simulated by using a sphere of high explosives to collapse eighteen small-scale models embedded in saturated sand.  Two basic types of models were used in the experiment,		

DD FORM 1473  
1 JAN 73

EDITION OF 1 NOV 65 IS OBSOLETE

UNCLASSIFIED

SECURITY CLASSIFICATION OF THIS PAGE (When Data Entered)

UNCLASSIFIED

SECURITY CLASSIFICATION OF THIS PAGE(When Data Entered)

20. ABSTRACT (Continued)  
symmetrical and asymmetrical. The symmetrical models represented pipe configurations used by the Defense Nuclear Agency (DNA) in their underground nuclear test program. They were designated as standard models. The results showed that all of these models produced high-energy jets. All other models contained some form of asymmetry on the inside surface of the model. The asymmetries were selected to either cause an off-axis collapse which would inhibit the formation of a jet, or to attenuate and suppress a jet after it is formed.

The results of the experiment show that high-energy jetting was present in all of the standard models, and was eliminated in the models with helical asymmetries. These findings continue to support the feasibility of using asymmetries to suppress jetting from the collapse of a pipe. However, their efficacy in a full-scale LOS pipe in an underground nuclear test environment cannot yet be postulated.

UNCLASSIFIED

SECURITY CLASSIFICATION OF THIS PAGE(When Data Entered)

## SUMMARY

A single laboratory experiment was performed to further evaluate the feasibility of using asymmetries to suppress jetting in line-of-sight (LOS) pipes that are collapsed by the ground shock from an underground nuclear test. Underground conditions were simulated by using a sphere of high explosives to collapse 18 small-scale models embedded in saturated sand.

Two basic types of models were used in this experiment, symmetrical and asymmetrical. The symmetrical models represented pipe configurations used by the Defense Nuclear Agency (DNA) in their underground nuclear test program. They were designated standard models. All other models contained some form of asymmetry on the inside surface of the model. The asymmetries were selected to either cause an off-axis collapse which would inhibit the formation of a jet, or to reduce the energy of a jet after it is formed.

The primary purpose of this study was to increase the experimental data base relating to the symmetrical and asymmetrical collapse of LOS models. The individual models were selected and grouped to support the following technical objectives:

- Assess the reproducibility of the jetting process from a standard LOS model.
- Assess the reproducibility of using a helical ribbon of polyolefin as an asymmetry to inhibit jetting.
- Investigate the effect of the type of material used for a helical asymmetry.
- Investigate the effect of the geometry of a polyolefin ribbon used as an asymmetry.
- Examine the effectiveness of using a relatively thick internal helix to reduce the energy in a jet after it is formed.
- Investigate the origin of jetting, the length and energy of the jet, and the efficacy of helical polyolefin ribbons for reducing high energy jets.
- Examine the jetting from a model representing a Pinex pipe and the effects of using a polyolefin helix to inhibit jetting.

With respect to these objectives, the major findings were as follow:

- All of the standard models produced high-energy jets. The jets produced deep craters in aluminum targets located at the end of the models. The target damage from four

identical standard models was not very reproducible. The mean crater depth was 5.4 cm, with a standard deviation of 1.7 cm. The mean crater volume was 23.3 cm<sup>3</sup>, and had a standard deviation of 14.3 cm<sup>3</sup>.

- All models with helical asymmetries eliminated high-energy jetting. However, the surfaces of the aluminum targets located at the end of these models were pitted with very small craters. The target damage from three identical models with helical asymmetries was quite reproducible.
- The material used for a helical asymmetry appears to be a relatively unimportant parameter. High-energy jets were eliminated with polyolefin, steel, and lead helices. While the target conditions from the three different materials were quite comparable, lead produced the least damage and steel produced the most damage to the surface of the target.
- The geometry of an asymmetry appears to be an important parameter. Unlike its helical counterpart, a polyolefin ribbon located on the inside surface of a model, but parallel to the model axis, produced a high-energy jet.
- A thick helical asymmetry, representing a baffle, was located beyond the collapse region of a LOS model, and produced the same results as a thin asymmetry located along the entire length of the model; high-energy jetting was eliminated and target damage was limited to very small craters on the surface of the target.

●Based on the depth and volume of craters produced in aluminum targets, a length of polyolefin helix located within the collapse region of a LOS model is more effective in reducing jet energy than removing the same length of model from the collapse process. These data indicate that jetting could be eliminated by a 25-cm length of polyolefin spiral, even though a much longer length of the model contributes to the jet formation. However, it should be noted that such dichotomous results may be due to the poor reproducibility of target damage from high-energy jets.

●The jet from a model used to simulate the collapse of a Pinex pipe was found to be more energetic than the jets from the models that were used to simulate a LOS pipe. Still, the jet was eliminated in a Pinex model with a helical ribbon of polyolefin on the inside surface of the model.

In addition to the findings given above, other important results were obtained from the penetration instrumentation that was included on the aluminum target of one of the standard models (No. 4). The data from this instrumentation provided the depth and velocity of the jet as it penetrated the target. The maximum depth of penetration was in good agreement with the post-test measurement. These data also showed that target penetration is initiated by jetted material which arrives at the target face with a velocity of approximately 0.6 cm/ $\mu$ s. This will have a significant impact on future modeling of the jetting process in LOS models since penetration was previously believed to be

initiated by the much faster material ( $\sim 1 \text{ cm}/\mu\text{s}$ ) that first arrives at the aluminum target.

Based on the results of this experiment, helical asymmetries can definitely be used to eliminate jetting in small-scale LOS models that are collapsed by a spherically divergent shock wave from a non-nuclear source. However, their efficacy in a full-scale LOS pipe, subjected to the complete environment of an underground nuclear test, cannot be postulated. Such use should only be considered after additional experimental and computational studies provide a better understanding of the jetting process and the effects of asymmetries. These studies should include numerical simulations of the present work, numerical simulations of the underground nuclear conditions, additional experiments to determine whether asymmetries inhibit the formation of a jet or reduce the energy of the jet after it is formed, and experiments to simulate more of the conditions in an underground nuclear test. Well-instrumented Pinex pipe experiments, with and without asymmetries, would be an excellent method for validating the concept of using asymmetries in an underground nuclear test environment. Successful results from such experiments would maximize the probability of success on a full-scale LOS pipe.

## TABLE OF CONTENTS

	<u>Page</u>
SUMMARY	1
LIST OF ILLUSTRATIONS	9
SECTION 1 INTRODUCTION	13
1.1 Background	13
1.2 Objectives	14
SECTION 2 DESCRIPTION OF EXPERIMENT (LS-3)	15
2.1 Concept	15
2.2 Experimental Apparatus	15
2.3 LOS Model Description	23
2.4 Measurements	35
SECITON 3 EXPERIMENTAL RESULTS	43
3.1 Detonation Wave	43
3.2 Shock Wave in Test Bed	43
3.3 Jet Velocity	46
3.4 Penetration	49
3.5 Target Damage	54
3.6 Summary of Results	72

PRECEDING PAGE BEGINS

## LIST OF ILLUSTRATIONS

<u>Figure</u>		<u>Page</u>
1.	Cross Section of LS-3 Experimental Configuration	16
2.	Plan View of LS-3 Experimental Configuration	17
3.	Explosive Source Used in LS-3	18
4.	Photograph of Typical LOS Model Used in LS-3	20
5.	(a) Photograph of Tank, Explosive Source, and LOS Models prior to Emplacement of Saturated Sand (LS-3); (b) Photograph of Tank and Aluminum Targets after Emplacement of Saturated Sand (LS-3)	22
6.	Basic Configuration of Standard Models 1, 2, 3, and 4 (LS-3)	25
7.	Basic Configuration of Poly Spiral Models 1, 2, and 3 (LS-3)	26
8.	Basic Configuration of Lead Spiral Model (LS-3)	28
9.	Basic Configuration of Steel Spiral Model (LS-3)	29
10.	Basic Configuration of Poly Strip Model (LS-3)	30
11.	Basic Configuration of Lead Baffle Model (LS-3)	31
12.	Basic Configuration of Standard Models with Standoffs (LS-3)	33
13.	Basic Configuration of Short Poly Spiral Models (LS-3)	34
14.	Basic Configuration of Pinex Standard Model (LS-3)	36
15.	Basic Configuration of Poly Spiral Model (LS-3)	37
16.	Configuration of Ionization Pins Used for Jet Velocity (LS-3)	39

LIST OF ILLUSTRATIONS (continued)

17.	Configuration of Pins Used for Measuring the Penetration in the Aluminum Target of Standard Model 4 (LS-3)	41
18.	Shock Trajectory in Saturated Sand of Experiment LS-3 from Diagnostic Line 1 (0°)	44
19.	Shock Trajectory in Saturated Sand of Experiment LS-3 from Diagnostic Line 2 (180°)	45
20.	Jet Velocities in Experiment LS-3 as Determined by Target Impact Switches Near Diagnostic Line 1 (0°)	47
21.	Jet Velocities in Experiment LS-3 as Determined by Target Impact Switches Near Diagnostic Line 2 (180°)	48
22.	Shock, Jet, and Penetration Trajectories for Experiment LS-3 and Standard Model 4	50
23.	Penetration of Aluminum Target by Standard Model 4 (LS-3)	51
24.	Trajectory and Velocity of Penetration in Aluminum Target by Standard Model 4 (LS-3)	53
25.	Cross Sections of Craters Produced in Aluminum Targets by the Standard Models in Experiment LS-3	56
26.	Surface of the Aluminum Targets from the Standard Models in Experiment LS-3	57
27.	Surface of the Aluminum Targets from the Poly Spiral Models in Experiment LS-3	59
28.	Surface of the Aluminum Targets from the Steel and Lead Spiral Models in Experiment LS-3	60
29.	Cross Section and Front Surface of the Aluminum Target from the Poly Strip Model in Experiment LS-3	61
30.	Surface of the Aluminum Target from the Lead Baffle Model in Experiment LS-3	62
31.	Cross Sections of Craters Produced in the Aluminum Targets by the Standard Models with Standoffs in Experiment LS-3	64
32.	Surface of Aluminum Targets from the Standard Models with Standoffs in Experiment LS-3	65
33.	Cross Sections of Craters Produced in Aluminum Targets by the Poly Spiral Models with Short Spirals in Experiment LS-3	66

LIST OF ILLUSTRATIONS (continued)

34.	Surface of Aluminum Targets from the Poly Spiral Models with Short Spirals in Experiment LS-3	67
35.	Penetration Produced in Aluminum Targets by LOS Models with Various Lengths of Polyolefin Spiral and Standoff Distances	68
36.	Volume of Crater Produced in Aluminum Targets by LOS Models with Various Lengths of Polyolefin Spiral and Standoff Distances	69
37.	Cross Section and Front Surface of the Aluminum Target from the Pinex Standard Model in Experiment LS-3	70
38.	Surface of the Aluminum Target from the Pinex Model with Poly Spiral in Experiment LS-3	71

# SECTION 1

## INTRODUCTION

### 1.1 BACKGROUND

Line-of-sight (LOS) pipes are frequently used in underground nuclear tests to collimate and transmit the radiation from a nuclear source to an experimental test station. The radiation is followed by a spherically divergent ground shock that causes the LOS pipe to collapse and form a high-energy jet. Occasionally, this jet constitutes a threat not only to the experimental objectives of the underground test, but also to the successful stemming and containment of the radioactive materials resulting from the test. The work reported here is part of the Defense Nuclear Agency's continuing effort to minimize the effects of jetting in LOS pipes, and thereby optimize the safety and data retrieval associated with their underground nuclear weapon effects testing program.

This report summarizes the results of a single experiment that was performed to investigate the jetting phenomena in small-scale LOS models. This experiment represents the final task of a program that was structured to evaluate the feasibility of using asymmetries to either inhibit the formation of jets or to reduce the severity of jets after they are formed. Experimental results from previous tasks indicated that helical ribbons of polyolefin or lead on the inside surface of a LOS pipe might be an effective

method of eliminating or suppressing jetting (Reference 1). The effectiveness of this method was demonstrated in an experiment using small, evacuated steel tubes (models) to simulate LOS pipes. Ten different LOS models were placed in a test bed of saturated sand and collapsed by the divergent shock wave from a sphere of high explosive. Jetting did not occur in the two models with internal helical asymmetries.

## 1.2 OBJECTIVES

The principal objective of the present work was to increase the experimental data base for small-scale LOS models that are collapsed by spherically divergent shock waves. Primary emphasis was placed on the reproducibility of the jetting/nonjetting phenomena associated respectively with the symmetrical/ asymmetrical collapse of the models. Secondary emphasis was directed at: (1) understanding the source of the jetting, (2) establishing whether internal asymmetries eliminate the cause, or suppress the results, of jetting, and (3) determining the sensitivity of specific asymmetry parameters on the collapse and jetting process.

## SECTION 2

### DESCRIPTION OF EXPERIMENT (LS-3)

#### 2.1 CONCEPT

A laboratory experiment designated as LS-3 was devised to simulate the conditions that exist during the collapse of a LOS pipe in an underground nuclear test. This experiment consisted of 18 small steel tubes positioned radially around a sphere of chemical high explosive and imbedded in saturated sand. The tubes, explosive, and sand were used to represent respectively the LOS pipes, the nuclear device, and the geological media in an underground nuclear test. The configuration of this experiment is shown schematically in Figures 1 and 2. A more complete description of the individual components of the experiment is given below.

#### 2.2 EXPERIMENTAL APPARATUS

2.2.1 Explosive Source. The explosive source is shown in Figure 3. Approximately 300 lbs (136 kg) of the liquid explosive nitromethane was contained in a two-foot-diameter fiberglass sphere. This explosive has a detonation pressure of 140 kb, comparable to the calculated peak free-field radial stress at a range of interest for a nuclear event such as MIGHTY EPIC.

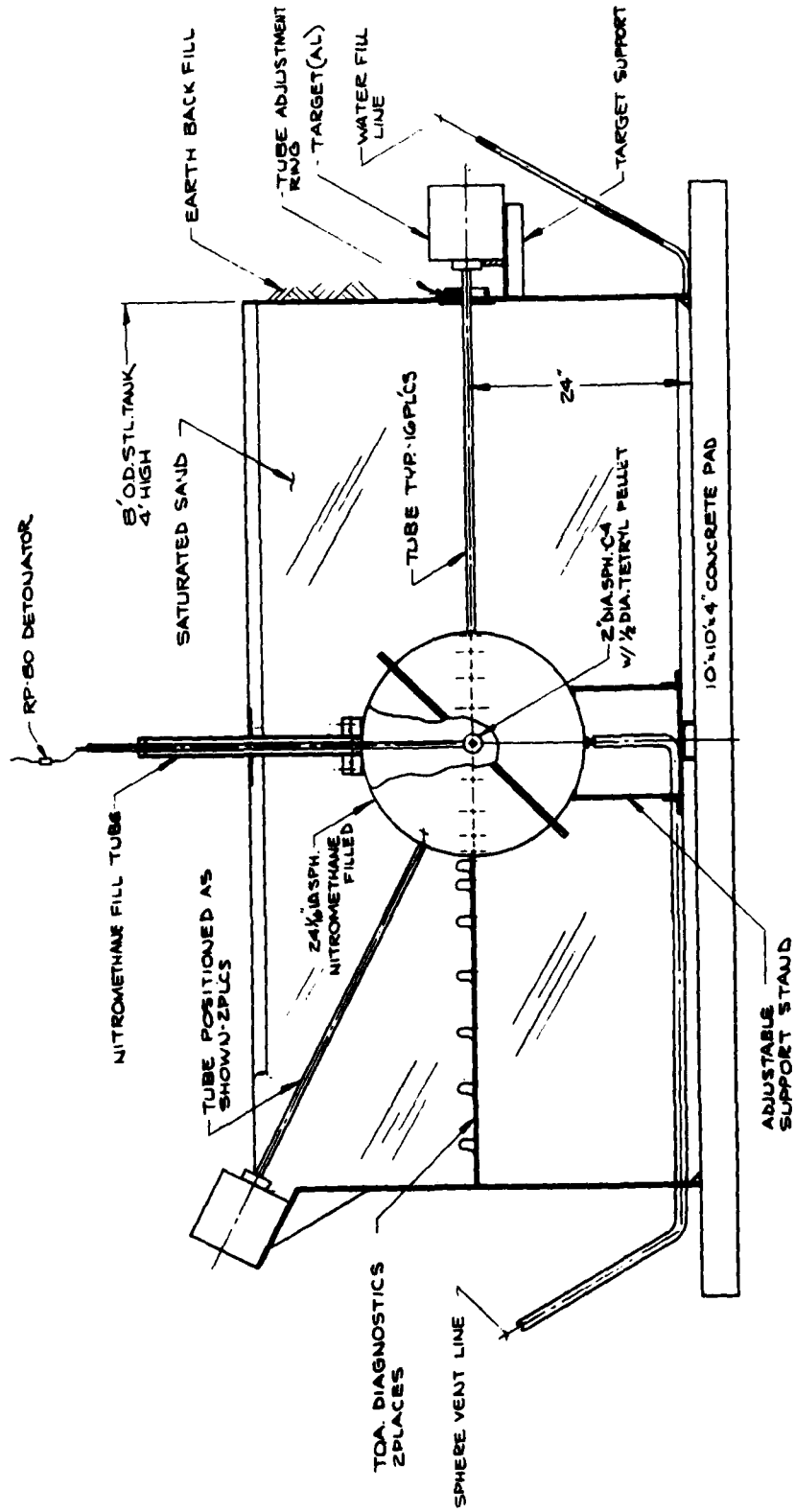


Figure 1 Cross section of LS-3 experimental configuration.

80-4-50

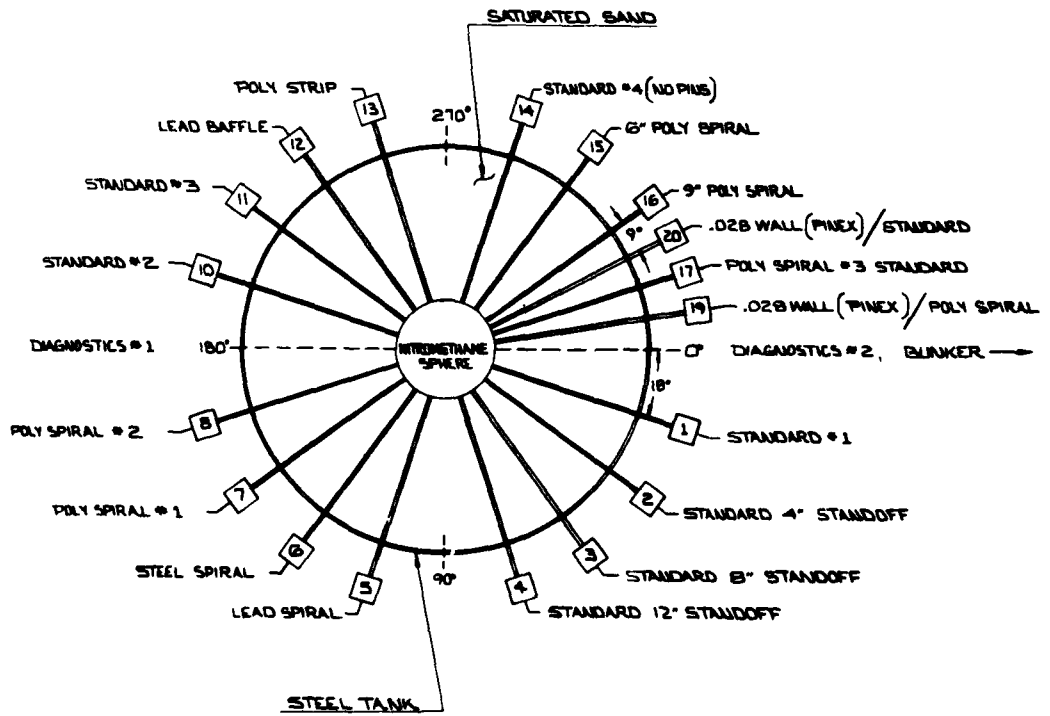


Figure 2 Plan view of LS-3 experimental configuration.



A booster assembly was used to initiate detonation in the nitromethane at the center of the sphere. It was placed into position through a vertical fill tube at the top of the sphere. The booster assembly was an explosive train consisting of a 1/2-inch- (1.25-cm-) diameter Tetryl pellet, and a length of mild detonating fuse which extended beyond the top of the fill tube. The detonation sequence in the explosive train was initiated by a RP-80 exploding bridge wire detonator located at the end of the fuse.

LOS Models. A typical LOS model is shown in Figure 1. The models were fabricated from 3/4-inch- (19-mm-) diameter welded and drawn AISI type 321 stainless steel tubes (Military Specification T-8808). All of the tubes had a wall thickness of 0.012 inch (0.305 mm) except for the two tubes used for the Pinex models, which had a wall thickness of 0.028 inch (0.71 mm). After the tubes were cut to the desired length, a steel plug was bonded onto the end of the tube facing the explosive sphere. An aluminum flange was bonded onto the opposite end of each tube. This flange was used to support a thin Mylar diaphragm and a vacuum port. Aluminum targets were then placed against the flange of each model. All of LOS models were evacuated to a pressure less than 1.0 mm Hg. The two Pinex models contained one atmosphere of air.

As shown in Figure 2, the models were designated either by title or their position around the explosive sphere. All of the LOS models were located in the horizontal midplane of the sphere. The two Pinex models were elevated above the midplane as illustrated in the cross-sectional view of Figure 1. All models

80-4-32

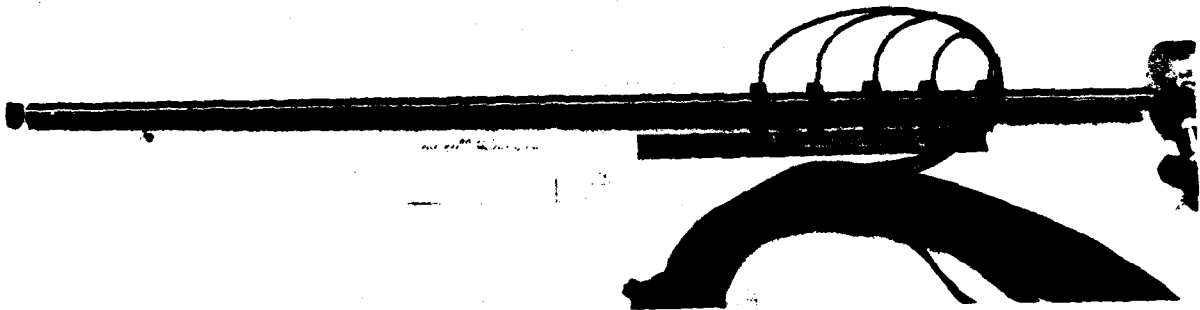


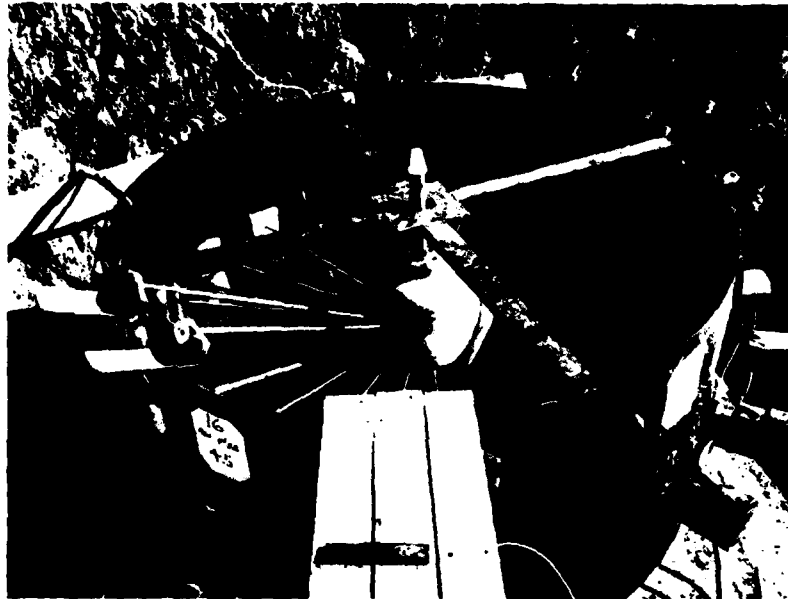
Figure 4 Photograph of typical LOS model used in LS-3.

were inserted into precisely located Lucite positioning rings on the surface of the explosive sphere and carefully aligned perpendicular to this surface.

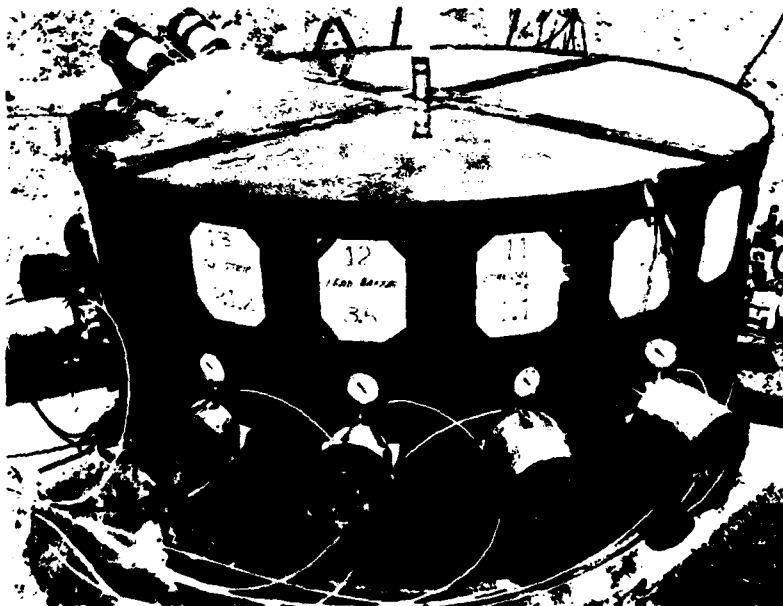
2.2.3 Test Bed. The saturated sand test bed was contained in a cylindrical steel tank. The tank was formed by rolling and welding a 1/4-inch- (6.4-mm-) thick steel plate into an 8-foot- (2.44-m-) diameter steel cylinder and reinforcing the top and bottom of the tank with U-channel. The tank was then placed on a concrete pad. The LOS models and instrumentation lines were positioned radially from the explosive sphere, which was located at the center of the tank. A photograph of these items appears in Figure 5a.

The test bed was prepared by carefully pouring sacks of Monterey sand into water which was controlled by a water distribution system around the perimeter of the bottom of the tank. The water distribution system consisted of perforated plastic tubing contained in a bed of pea-sized gravel. Care was taken to maintain a thin slurry of sand and water in the tank at all times. The slurry was mixed by hand to assure thorough wetting of the sand grains and to avoid trapping air bubbles. Figure 5b is a photograph of the experimental setup after the tank has been filled with sand.

The instrumentation for determining the time-of-arrival of the shock wave in the saturated sand was located at positions 0° and 180° (Figure 2). In a similar manner, the horizontal plane of positions 90° and 180° contained the flange joint for



(a)



(b)

80-4-33

Figure 5 (a) Photograph of tank, explosive source, and LOS models; (b) photograph of tank and aluminum targets after emplacement of saturated sand (LS-3).

the two fiberglass hemispheres that formed the explosive sphere. The flange was oriented at a 45° angle with respect to the horizontal plane.

### 2.3 LOS MODEL DESCRIPTION

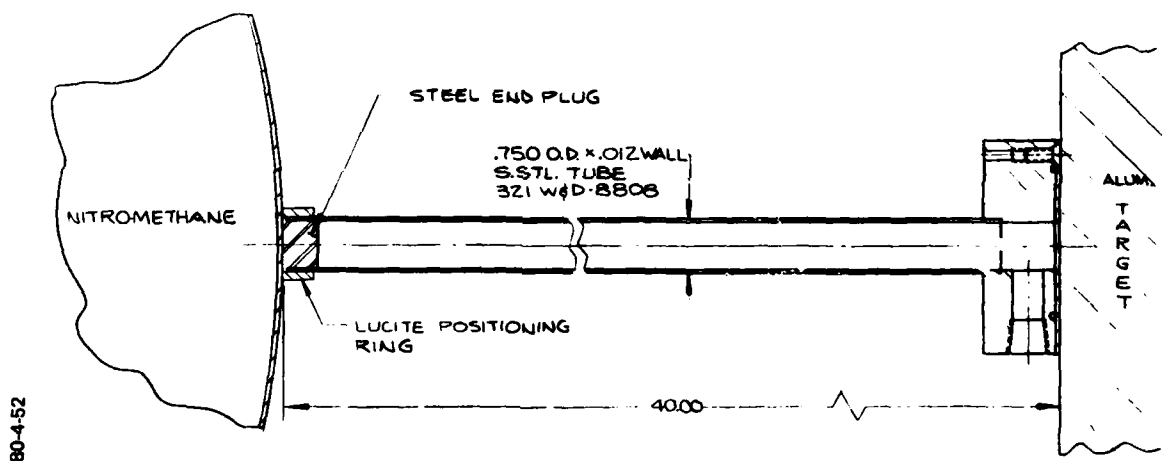
The LOS models used in this experiment are listed in Table 1. This table provides a brief description of each model, its position in the test bed, the relevant dimensions of the model, and the salient dimensions of any asymmetries that were included in the model. It also denotes any instrumentation that was used for the model. The 18 models can be categorized according to technical objective in the following manner:

2.3.1 Reproducibility of Standard Models. Models without asymmetries were designated as Standard and represented LOS pipe configurations used by DNA in their underground nuclear test program. Four of these models were included to establish the reproducibility of the jetting phenomena from models that are collapsed symmetrically onto their axis. Standard Models 1, 2, 3, and 4, similar to that shown in Figure 6, were located respectively in positions 1, 10, 11, and 14 around the explosive sphere.

2.3.2 Reproducibility of Polyolefin Spiral Models. A thin polyolefin ribbon was located on the inside surface of these LOS models, as shown in Figure 7. Each ribbon was positioned to form a helix (spiral) with a 2-inch (50.8-mm) pitch which would introduce asymmetries into the collapse process along the entire length of the model. Three of these models, Poly Spiral Models

Table 1 Description of LOS models used in experiment LS-3.

MODEL DESIGNATION	MODEL POSITION	STAINLESS STEEL TUBE 19 mm O.D.		SPIRAL TYPE					NOTES
		Length (mm)	Wall Thk. (mm)	Mat'l	Width (mm)	Thk. (mm)	Length (mm)	Pitch (mm)	
Standard No. 1	1	993.8	0.305	--	--	--	--	--	TOA instrumentation on model and target face
Standard--4" Standoff	2	892.2	0.305	--	--	--	--	--	Tube began 101.6 mm (4 in.) from explosive sphere
Standard--8" Standoff	3	790.6	0.305	--	--	--	--	--	Tube began 203.2 mm (8 in.) from explosive sphere
Standard--12" Standoff	4	689.0	0.305	--	--	--	--	--	Tube began 304.8 mm (12 in.) from explosive sphere
Lead Spiral	5	993.8	0.305	Lead	12.7	0.330	982.7	50.8	
Steel Spiral	6	993.8	0.305	Steel	15.9	0.457	982.7	50.8	
Poly Spiral No. 1	7	993.8	0.305	Poly-olefin	12.7	0.406	982.7	50.8	
Poly Spiral No. 2	8	993.8	0.305	Poly-olefin	12.7	0.406	982.7	50.8	
Standard No. 2	10	993.8	0.305	--	--	--	--	--	Same as Standard No. 1
Standard No. 3	11	993.8	0.305	--	--	--	--	--	Same as Standard No. 1
Lead Baffle	12	993.8	0.305	Lead	3.18	3.18	384.2	50.8	Spiral positioned 609.6 mm (24 in.) from explosive sphere
Poly Strip	13	993.8	0.305	Poly-olefin	12.7	0.406	982.7	"	Strip parallel to tube axis
Standard No. 4	14	993.8	0.305	--	--	--	--	--	Penetration pins and carbon gage in target
Poly Spiral--6" Spiral	15	993.8	0.305	Poly-olefin	12.7	0.406	152.4	50.8	Spiral located inside first 152.4 mm (6 in.) of the tube
Poly Spiral--9" Spiral	16	993.8	0.305	Poly-olefin	12.7	0.406	228.6	50.8	Spiral located inside first 228.6 mm (9 in.) of the tube
Poly Spiral No. 3	17	993.81	0.305	Poly-olefin	12.7	0.406	982.7	50.8	
Pinex-Poly Spiral	19	993.8	0.710	Poly-olefin	12.7	0.406	982.7	50.8	Larger wall thickness and one atmosphere of air
Pinex-Stanoaro	20	993.8	0.710	--	--	--	--	--	Larger wall thickness and one atmosphere of air



80-4-52

Figure 6 Basic configuration of Standard Models 1, 2, 3, and 4 (LS-3).

80-4-53

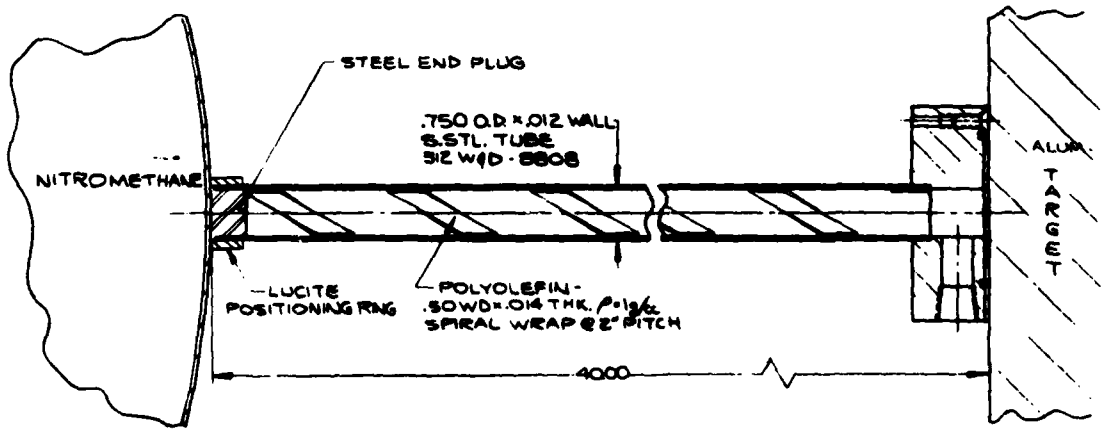


Figure 7 Basic configuration of Poly Spiral Models 1, 2, and 3 (LS-3).

1, 2, and 3, were used to determine the reproducibility of their jet suppression properties and were located respectively in positions 7, 8, and 17 around the sphere.

2.3.3 Effect of Materials. Except for the materials, width and thicknesses used for the helix, the Lead Spiral Model and Steel Spiral Model were identical to the Poly Spiral Models. The configurations for these models are given respectively in Figures 8 and 9. They were included to examine the effect of the type of material used for an asymmetry. They were located in positions 5 (Lead) and 6 (Steel).

2.3.4 Effect of Geometry. The polyolefin ribbon used in the Poly Strip Model was the same as used on the Poly Spiral Models. However, it was positioned on the inside surface of the model parallel to the model's axis as shown in Figure 10. In effect, it was a spiral with an infinite pitch, included to investigate the geometrical effect of an asymmetry. This model was located in position 13.

2.3.5 Effect of a Baffle. The Lead Baffle Model was included to examine the effect of a spiral on a jet after it is formed. A thick lead spiral (baffle) was placed on the inside surface of the model as shown in Figure 11. The baffle was located 24 inches (609.6 mm) from the surface of the explosive sphere, and extended to the end of the model nearest the aluminum target. In this position, the jet was expected to be fully formed before entering the baffle section.

80-4-54

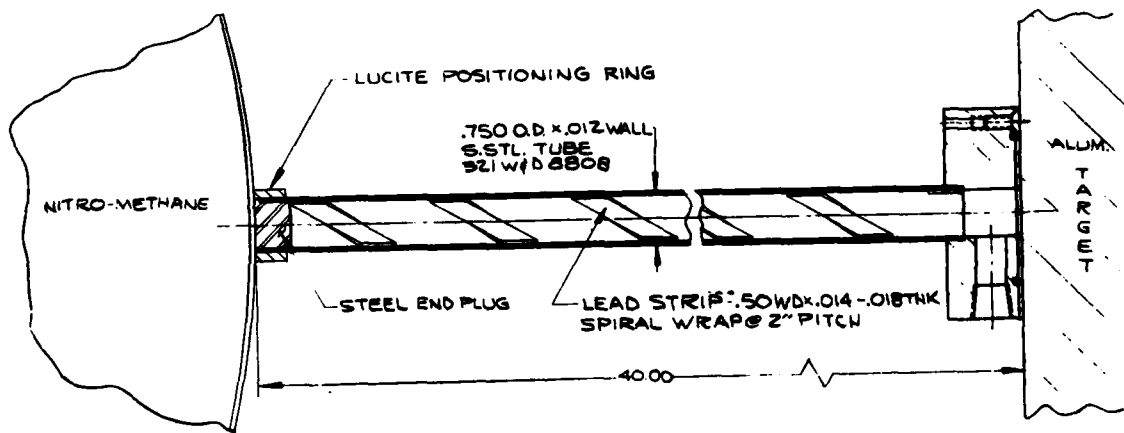
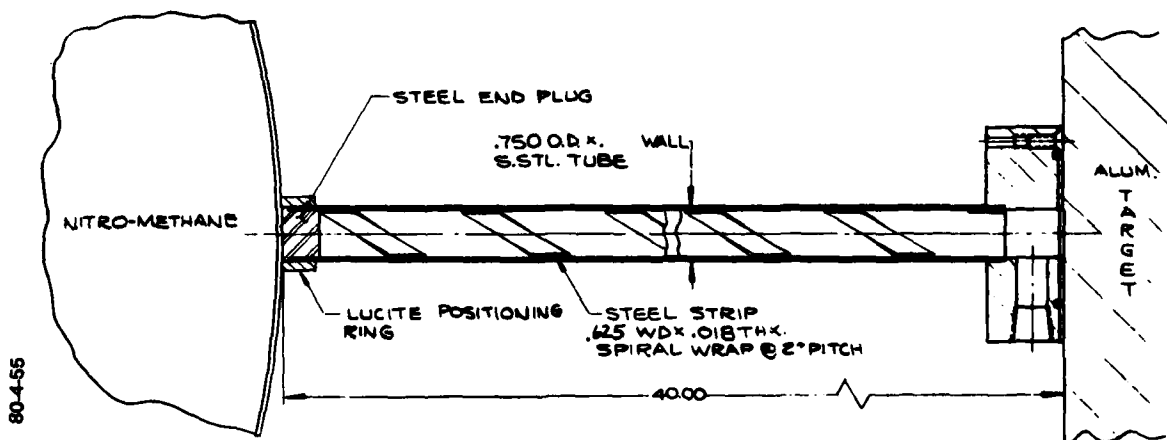


Figure 8 Basic configuration of Lead Spiral Model (LS-3).



80-4-55

Figure 9 Basic configuration of Steel Spiral Model (LS-3).

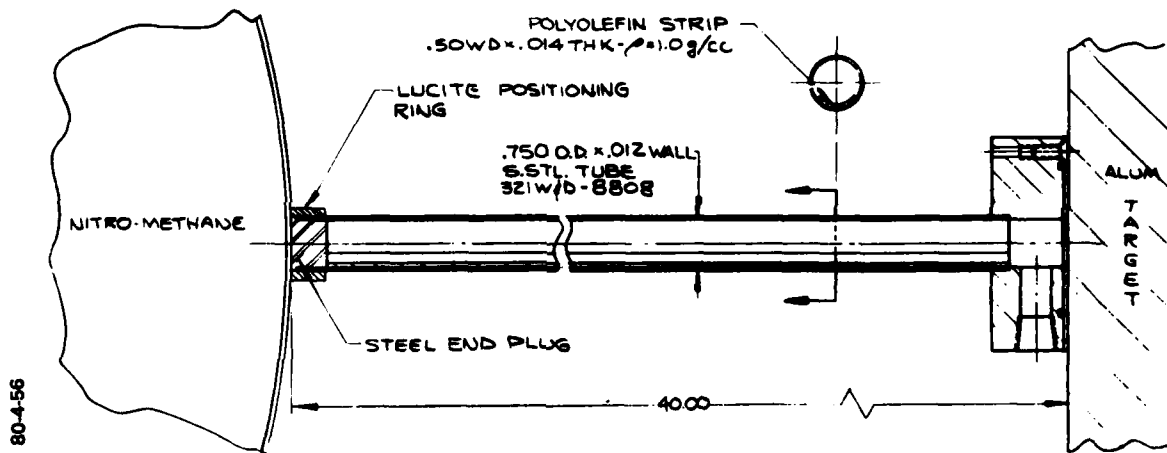
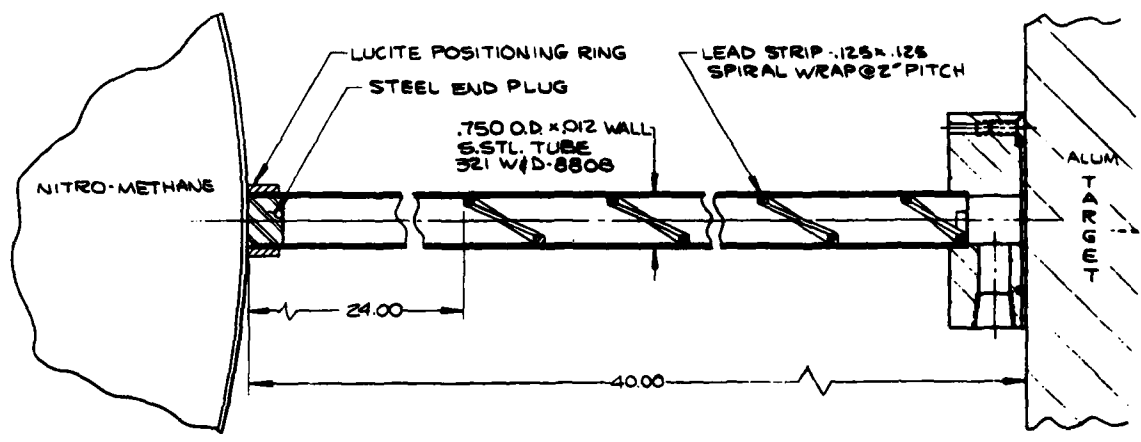


Figure 10 Basic configuration of Poly Strip Model (LS-3).



80-4-57

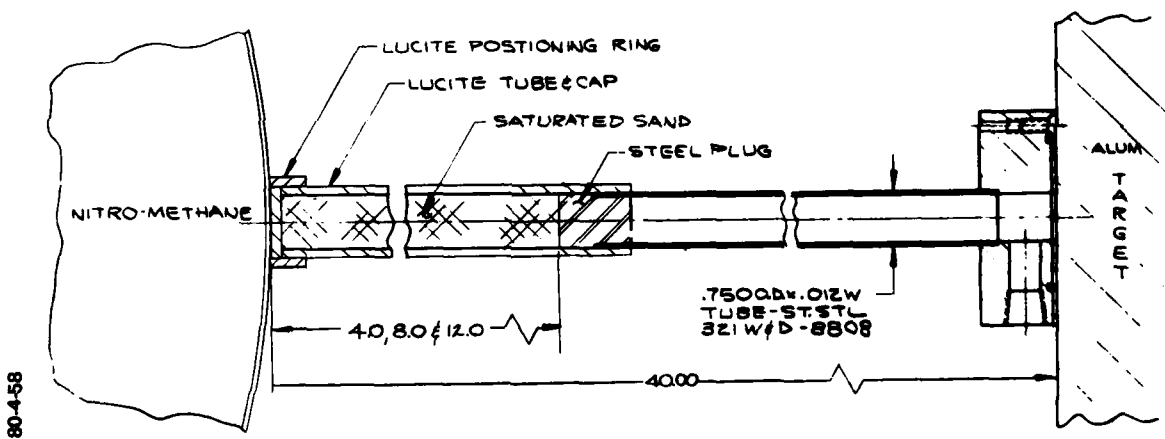
Figure 11 Basic configuration of Lead Baffle Model (LS-3).

2.3.6 Source Resolution. The models in this category were included to provide a larger data base on the source of jetting and the mechanisms by which jets are suppressed by internal spirals.

The three Standard Models with Standoffs were expected to yield additional information about the origin, extent, and limits of jetting. The models were placed at three different distances from the sphere of explosive as shown in Figure 12. Sand-filled Lucite tubes were used as spacers between the end of the models and the explosive sphere. The distance between the sphere and the aluminum targets was the same as all other models. The standoff distances for the three models were 4 inches (101.6 mm), 8 inches (203.2 mm), and 12 inches (304.8 mm). They were located respectively in positions 2, 3, and 4 around the sphere.

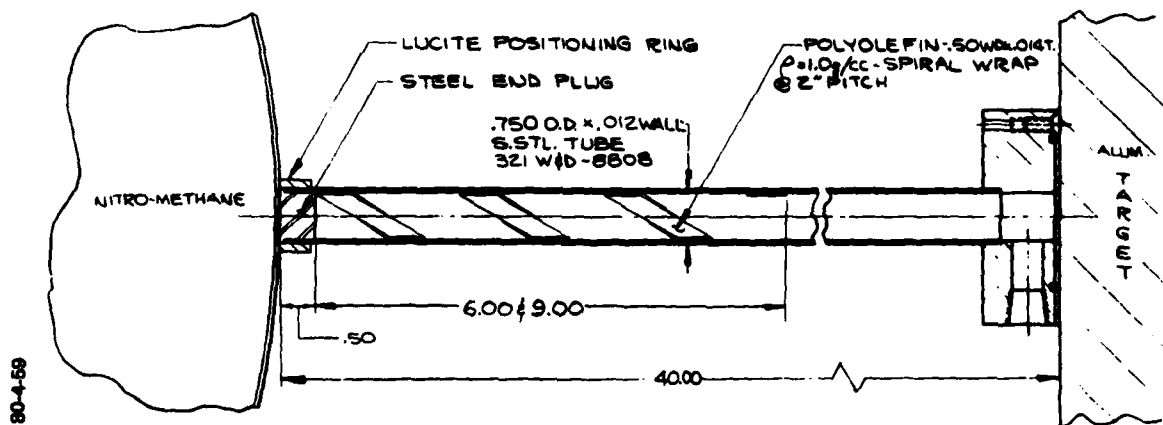
Further discrimination of the jet suppression characteristics of internal spirals was expected from the two Poly Spiral Models with shorter spirals. These models had polyolefin spirals that extended 6 inches (152.4 mm) and 9 inches (228.6 mm) from the end plug in the model as shown in Figure 13. They were located respectively in positions 15 and 16 around the sphere. These models were included to investigate the location and axial extent of jetting, and to help differentiate whether or not the internal asymmetries affected the formation of jets or suppressed them after they are formed.

2.3.7 Simulation of Pinex Pipe. These models were included to investigate the effect that an asymmetry would have on a Pinex pipe. In order to realistically simulate the parameters used in a Pinex experiment, the wall thickness of these models was increased



80-458

Figure 12 Basic configuration of Standard Models with Standoffs (LS-3).



80-4-59

Figure 13 Basic configuration of Short Poly Spiral Models (LS-3).

to 0.028 inch (0.71 mm), and they were tested with one atmosphere of air in the models. The Pinex-Standard Model had no asymmetry and served as a control model (Figure 14). The Pinex-Poly Spiral Model had a polyolefin helix along the entire length as shown in Figure 15. These models were located respectively in positions 19 and 20. It should be noted that, unlike all other models, they were located in a plane 26° above the horizontal plane containing all of the other models.

## 2.4 MEASUREMENTS

The active instrumentation used in this experiment was directed at determining the time at which the detonation reaches the inside surface of the fiberglass sphere, the trajectory of the spherically divergent shock wave in the saturated sand, the velocity of the jets generated in six of the LOS models, and the rate at which the jet penetrates the aluminum target of one of the standard models. A carbon stress gage was also embedded in the target that was instrumented for penetration.

Aluminum targets were placed at the end of all models to provide passive, terminal evidence of the energy and momentum contained in the jet.

2.4.1 Detonation Wave. Two ionization pins were located on opposite sides of the explosive sphere. They were positioned on the inside surface of the fiberglass sphere to measure the time at which the detonation wave reaches this interface. The purpose of this measurement was to assure that the detonation was spherically symmetrical about the point of initiation prior to entering the saturated sand surrounding the models.

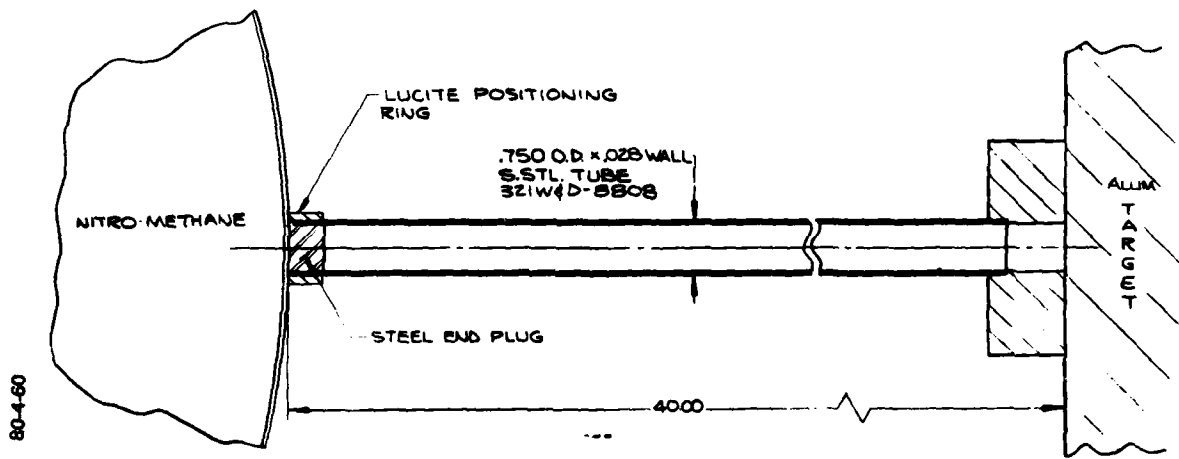


Figure 14 Basic configuration of Pinex Standard Model (LS-3).

80-4-61

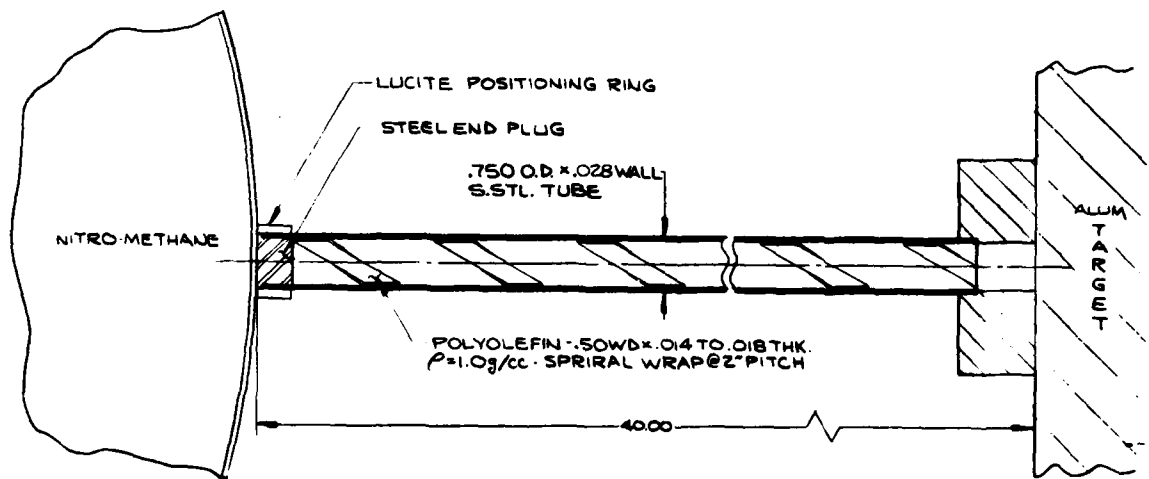


Figure 15 Basic configuration of Pinex Poly Spiral Model (LS-3).

2.4.2 Shock Wave in Test Bed. The trajectory of the spherically divergent shock wave in the saturated sand test bed was determined from time-of-arrival measurements. These measurements were obtained from the response of two radial lines of seven piezoelectric pins that were placed in the saturated sand on opposite sides of the explosive sphere. They were located in the horizontal midplane of the sphere and extended from 32 cm to 107 cm from the center of the sphere. The first piezoelectric pin of each radial line was located 1.5 cm from the inside surface of the explosive sphere. The intervals between the first and second pin and between the second and third pin were 5 cm and 10 cm, respectively. Thereafter the interval between pins was 15 cm.

2.4.3 Jet Velocity. Instrumentation for determining jet velocity was included on three of the four standard models (Positions 7, 8, and 17). The instrumentation consisted of five ionization pins placed through the walls of the models at 5-cm intervals, and extending from 65 cm to 85 cm from the steel plug on the end of the model nearest to the explosive sphere. The geometry for the ionization pin instrumentation is shown in Figure 16. The pins can also be seen in the photograph of the LOS model presented in Figure 4.

In addition to the ionization pins, each of the above models had impact switches adjacent to the aluminum targets on the flange end of the model. These switches consisted of two aluminum foils separated by a thin Mylar film. When penetrated by a jet, they close an electrical circuit, thus providing the time at which the leading edge of the jet arrives at the aluminum target.

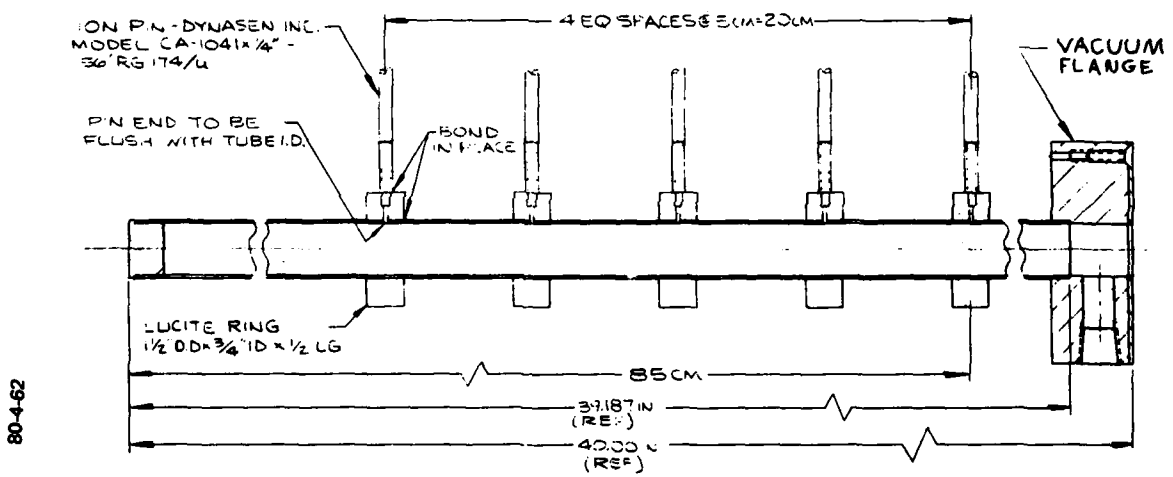
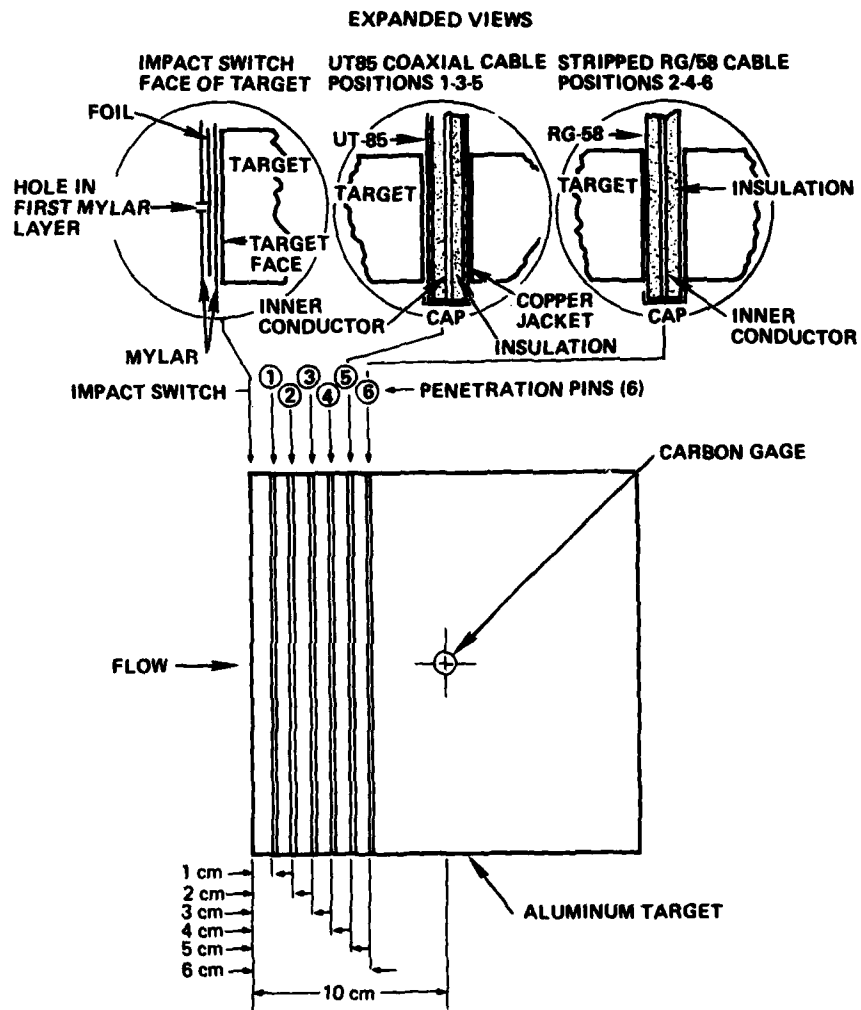


Figure 16 Configuration of ionization pins used for jet velocity (LS-3).

2.4.4 Target Penetration. As shown in Figure 17, the 6061-T6 aluminum target used for Standard Model No. 4 (Position 14) contained two different sets of time-of-arrival (TOA) instrumentation to investigate the rate at which the jet penetrates the aluminum. One set consisted of three UT 85 coaxial cables that were located 1, 3, and 5 cm from the front face of the target. The pins were placed into small tight-fitting holes drilled through the centerline of the target. The other set of TOA instrumentation was constructed by stripping the outer conductor from three RG-58 coaxial cables. The stripped cables were also inserted through small holes at the centerline of the target. The holes were located 2, 4, and 6 cm from the front face of the aluminum target. The time-of-arrival of the jet at the aluminum target was obtained using the impact switch located on the face of the target.

This target also contained a 505-ohm, 2-watt carbon resistor that was used as a pressure gage. An aluminum-filled epoxy was used to bond the 0.39-inch (9.9-mm) resistor in the aluminum target. While the gage was not calibrated directly, the sensitivity was calculated to be approximately 110 mV per kilobar based on the pressure-resistance properties of carbon (~ 5% resistance change per kilobar of pressure) and the electrical circuit used.

2.4.5 Target Damage. The character, depth, and diameter of the craters produced in aluminum targets located at the end of each model were used to provide terminal evidence of the energy and momentum in the jets. The targets were 6061-T6 aluminum cylinders, 8 inches (20.3 cm) long and 8 inches (20.3 cm) in diameter. They were placed on brackets welded to the outside of the steel test bed tank and positioned as close as possible to the vacuum flange and Mylar diaphragm that enclosed one end of each model.



80-4-63

Figure 17 Configuration of pins used for measuring the penetration in the aluminum target of Standard Model 4 (LS-3).

## SECTION 3

### EXPERIMENTAL RESULTS

#### 3.1 DETONATION WAVE

The two ionization pins on the inside surface of the fiberglass sphere showed a 0.4- $\mu$ s difference in the times at which the detonation wave arrived on opposite sides of the sphere. This measurement indicates that the detonation was not perfectly symmetric about the point of initiation. Assuming the detonation velocity in the nitromethane was 0.6 cm/ $\mu$ s, a 0.4- $\mu$ s difference in arrival time would imply that the detonation wave on one side of the sphere was leading the opposite side by 0.24 cm. Since the fiberglass sphere had an internal radius of 30.6 cm, this represents a difference of 0.78 percent. This difference is probably due to the inability to maintain the shape of the thin-walled fiberglass sphere when it is filled with 300 pounds (136 kg) of a liquid and covered with saturated sand. Therefore, for all practical purposes, the detonation was quite symmetrical.

#### 3.2 SHOCK WAVE IN TEST BED

The time-of-arrival data for the spherically divergent shock wave along Diagnostic Line No. 1 (0° position) in the saturated sand are given in Figure 18. Comparable data for Diagnostic Line No. 2 (180° position) are shown in Figure 19. Individual data points are given for each piezoelectric pin. If a pin reported more than once, all data are given. It should also be noted that

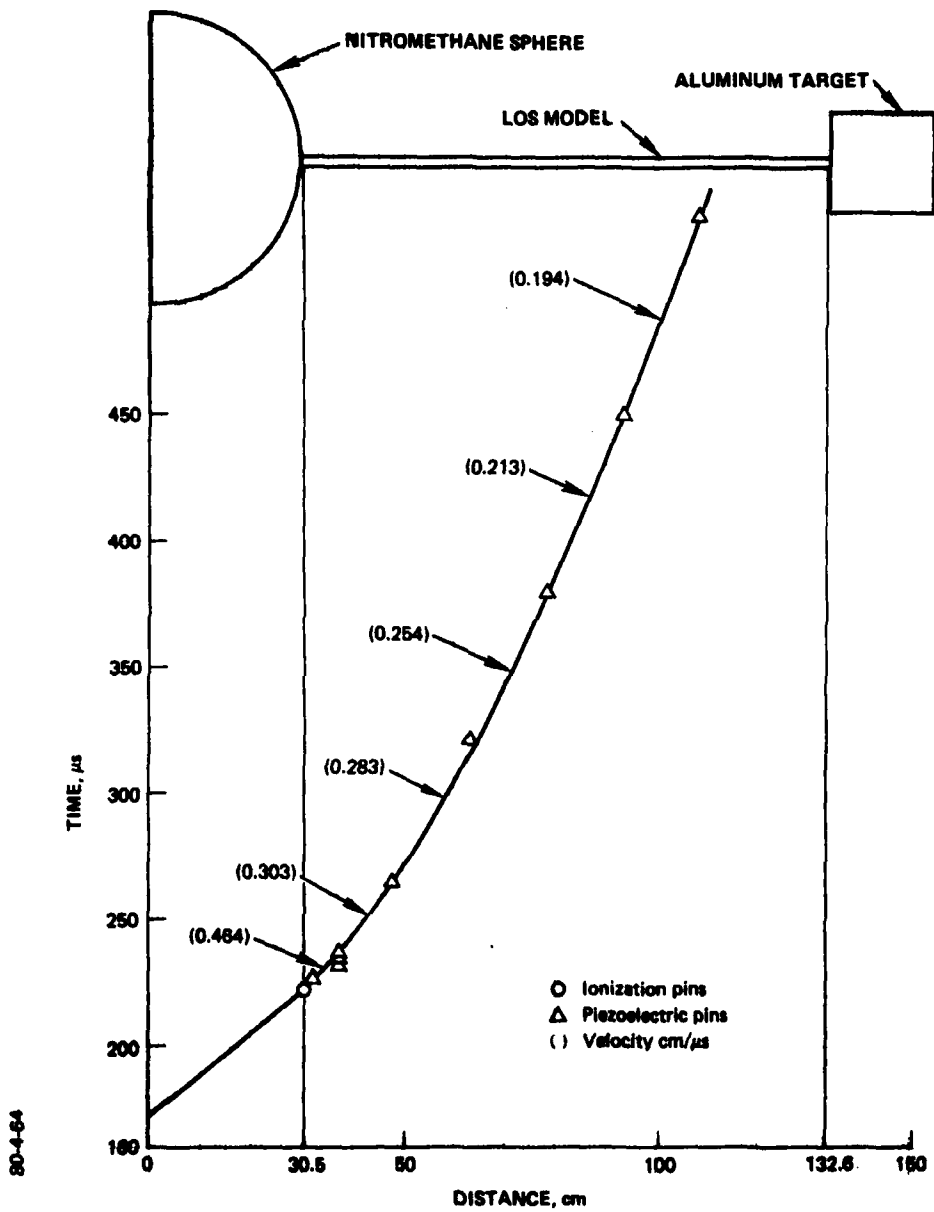


Figure 18 Shock trajectory in saturated sand of Experiment LS-3 from diagnostic line 1 ( $0^\circ$ ).

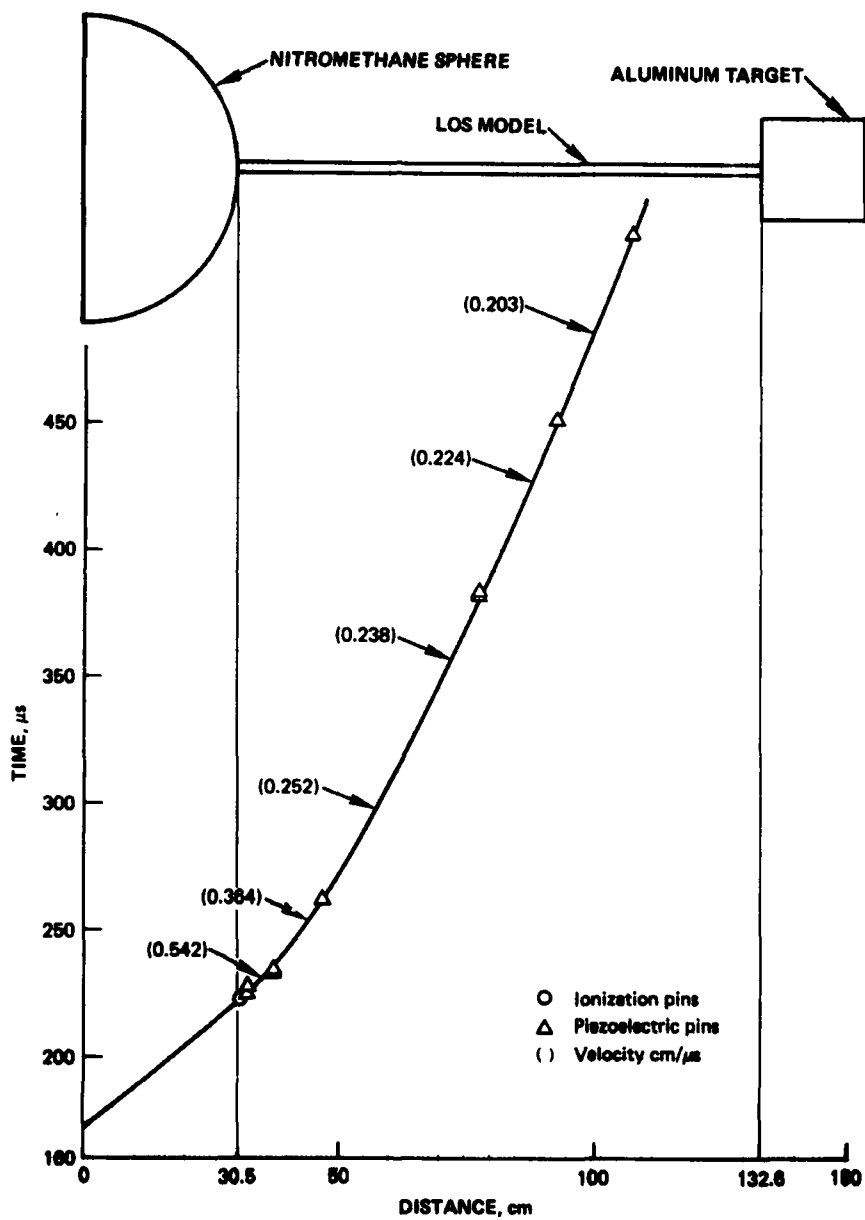


Figure 19 Shock trajectory in saturated sand of Experiment LS-3 from diagnostic line 2 ( $180^\circ$ ).

separate tests of initiation systems identical to the one used for this experiment [RP-80 detonator and 48 inches (121.9 cm) of mild detonating fuse] provided the booster detonation time of 172  $\mu$ s at the center ( $x = 0$ ) of the explosive sphere. The agreement between the two diagnostic lines is quite good. The slope of the smooth curve provides the shock velocity in the sand as a function of distance from the explosive source. The shock velocity on the surface of the sphere is in the range of 0.3 cm/ $\mu$ s to 0.5 cm/ $\mu$ s, indicating a high degree of water saturation in the sand.

### 3.3 JET VELOCITY

The time-of-arrival data obtained from the ionization pins located in the sidewalls of the three Standard Models and the three Poly Spiral Models were uninterpretable. We believe that the epoxy used to bond and seal the coaxial pins to the walls of the models accumulated on the open ends of the pins. The resulting insulation between the inner and outer electrodes either prevented or delayed prompt electrical closure of the pin circuit.

The velocity of the jets produced by the collapse of the various LOS models can be inferred from the time at which the jet closes the impact switch at the end of the model. These data are presented in Figures 20 and 21. The times-of-arrival at the impact switch for the various models have been added to the shock wave trajectories from the diagnostic line closest to the models. The origin of the leading edge of the jet is postulated to be on the axis of the model adjacent to the explosive sphere. The jet would be formed 5  $\mu$ s (time for collapse) after the shock

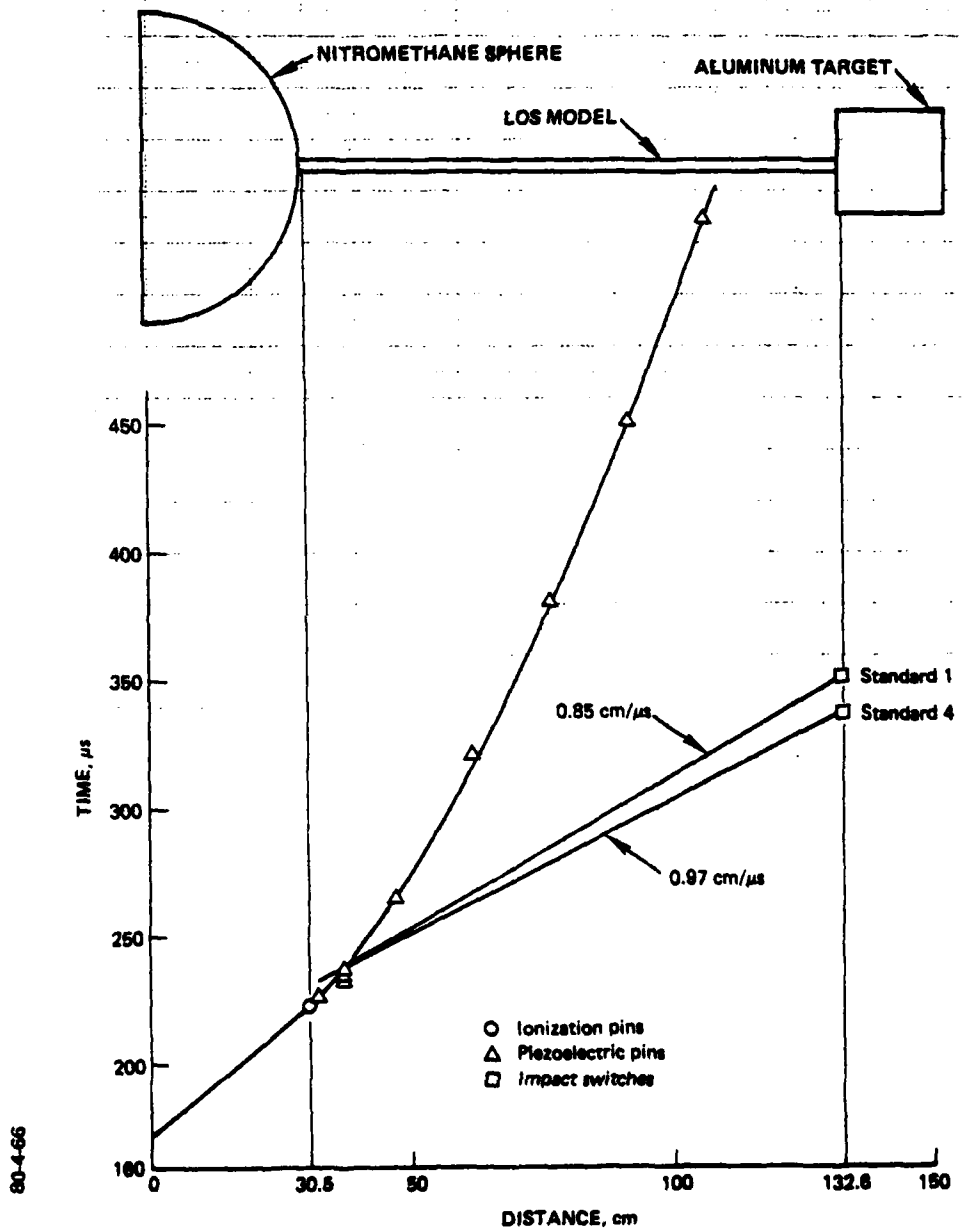


Figure 20 Jet velocities in Experiment LS-3 as determined by target impact switches near diagnostic line 1 ( $0^\circ$ ).

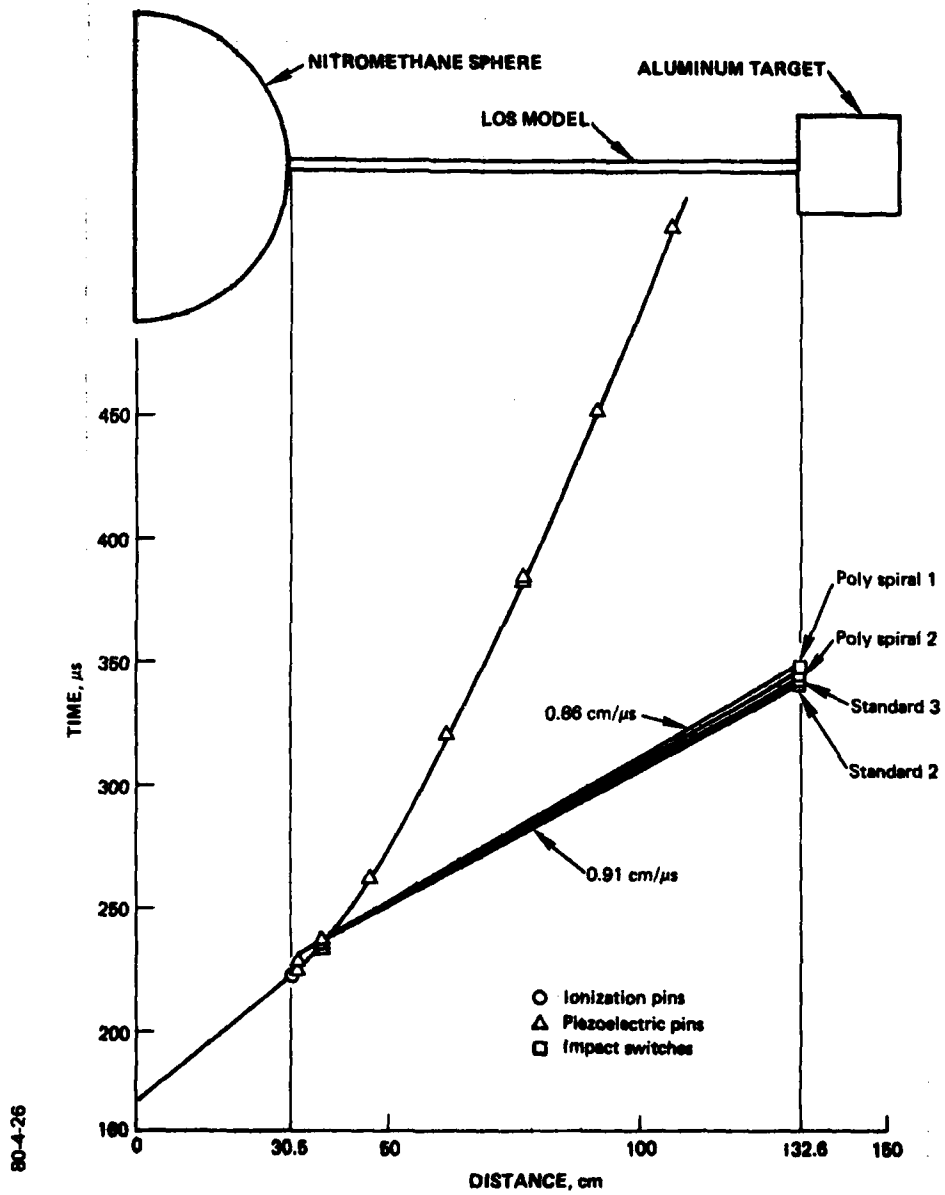


Figure 21 Jet velocities in Experiment LS-3 as determined by target impact switches near diagnostic line 2 ( $180^{\circ}$ ).

in the saturated sand passes over that axial location. A straight line between this jet origin and the impact switch times provides a reasonable estimate of the leading edge of the jet. As shown in Figure 20, the jet velocities were 0.85 cm/ $\mu$ s and 0.97 cm/ $\mu$ s, respectively, for Standard Models 1 and 2, located near Diagnostic Line #1. Comparable velocities were obtained for Standard Models 2 and 3 and Poly Spiral Models 1 and 2, located near Diagnostic Line #2 (Figure 21).

#### 3.4 PENETRATION

The results from the penetration measurements on Standard Model No. 4 were quite surprising. The times at which the jet closed the various penetration pins along the axis of the aluminum target are shown in Figure 22. This figure also shows the time at which the leading edge of the jet reached the face of the target. There is a difference of 61  $\mu$ s between the first arrival and the initiation of penetration. Furthermore, a straight line between the postulated origin of the jet and the onset of penetration yields a velocity of 0.62 cm/ $\mu$ s. These results indicate that the leading edge of the jet is very tenuous and possesses very little energy or momentum. Furthermore, the target is penetrated by jet material moving at a velocity of 0.62 cm/ $\mu$ s instead of the 0.97 cm/ $\mu$ s indicated by the impact switch.

The dynamics of the penetration are shown more clearly in Figure 23. Here, the time-of-arrival data from the first five pins are plotted as a function of depth into the aluminum target. A smooth curve through the data points defines the trajectory of the front edge of the penetration, which appears to

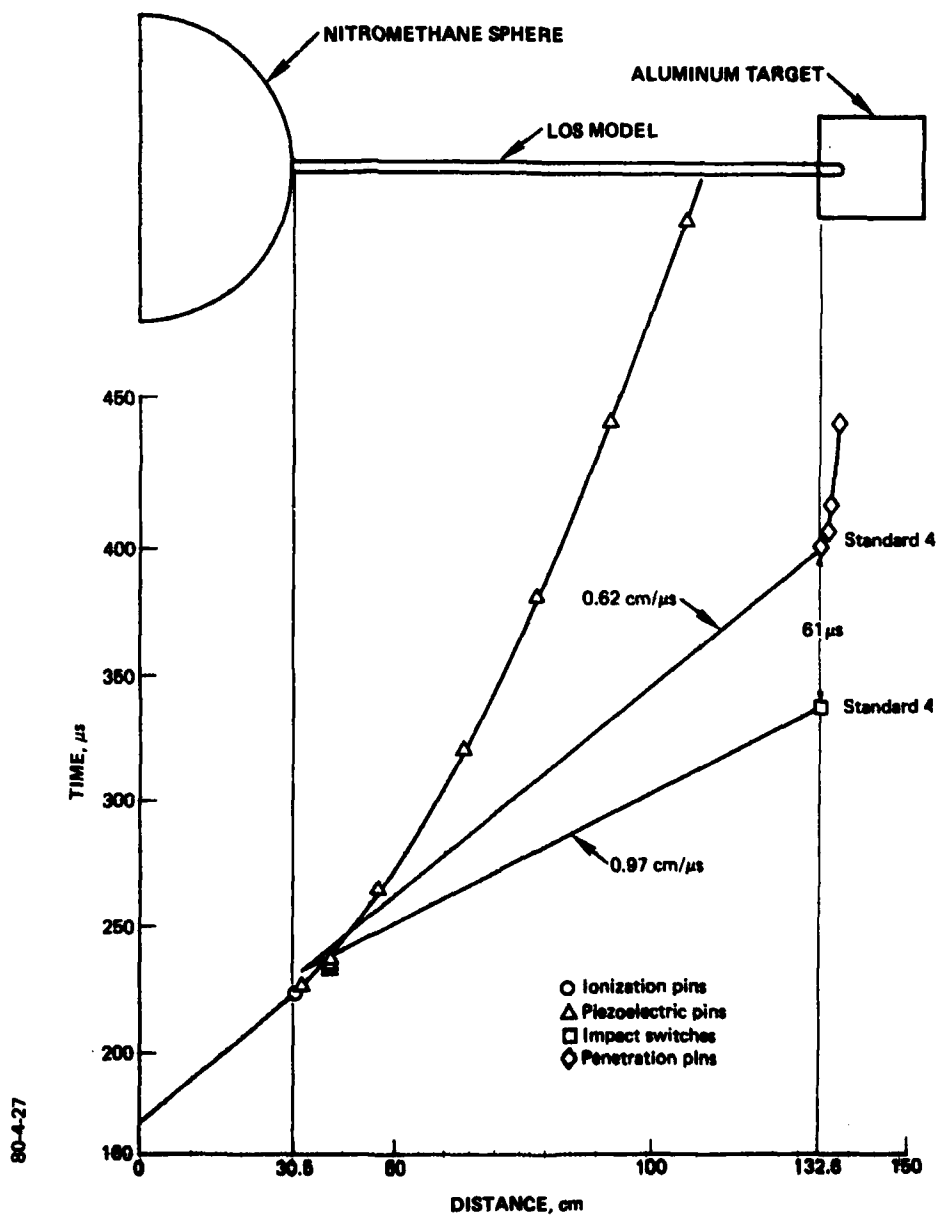


Figure 22 Shock, jet, and penetration trajectories for Experiment LS-3 and Standard Model 4.

80-4-28

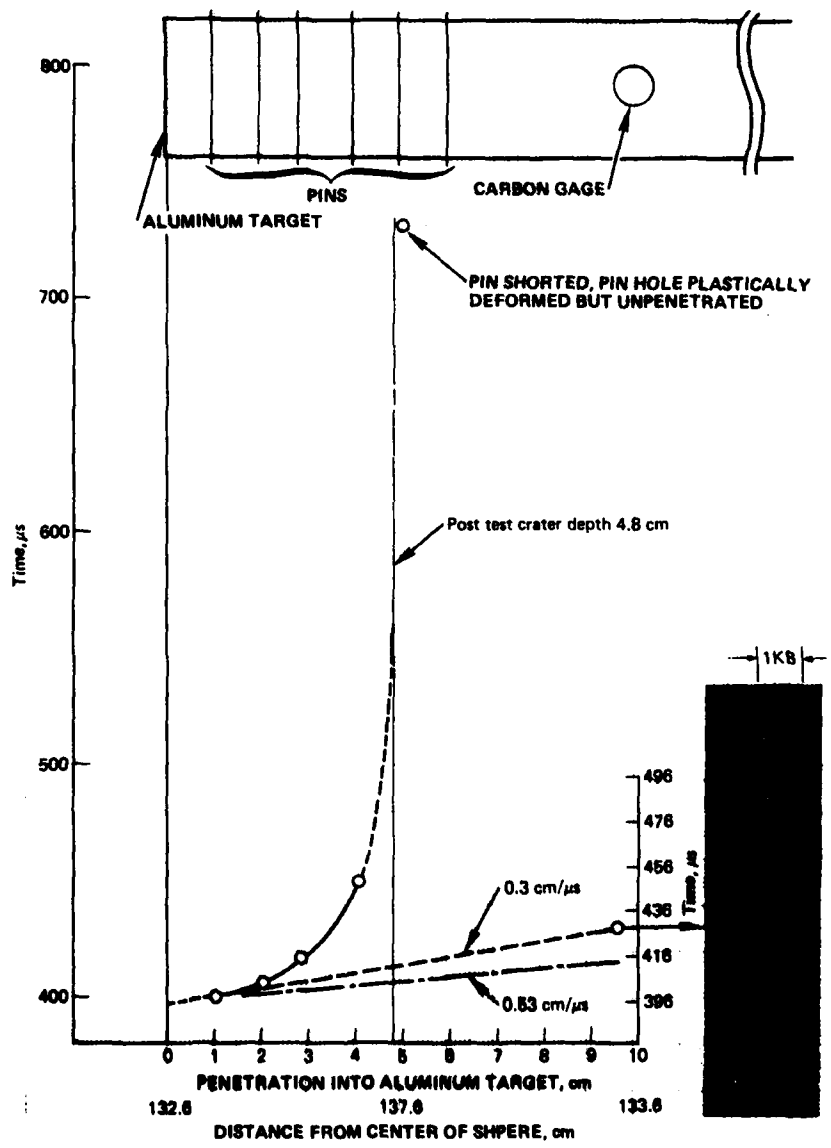


Figure 23 Penetration of aluminum target by Standard Model 4 (LS-3).

reach an asymptote that is approximately equal to the post-test measurement of 4.8 cm. It should be noted that the penetration pin located at  $x = 5$  cm provided a time-of-arrival signal. However, post-test examination showed that the pin had been plastically deformed but had not been penetrated.

An oscilloscope record from the carbon resistor gage is presented on the right-hand side of Figure 23. Unfortunately, the stress signature in the aluminum target is obscured by high-frequency electrical noise. However, the noise appears to occur in bursts at times corresponding to the response of the impact switch and the penetration pins. Furthermore, the frequency and character of the record appear to change near the center of the record. If an elastic stress wave were moving through the aluminum target at the unrealistically low velocity of  $0.3 \text{ cm}/\mu\text{s}$ , this could be interpreted as the arrival of the wave at the gage location. If this were the case, the peak amplitude would indicate a pressure of approximately 1 kb.

The penetration data given in Figure 23 can be fitted with an equation of the form

$$x = p \left( \frac{\frac{t}{\tau}}{1 + \frac{t}{\tau}} \right)$$

where  $p$  is the penetration depth at  $t = \infty$  or 4.8 cm for this target. A value of  $\tau = 11.5 \mu\text{s}$  gives a good fit to the early penetration, as shown by Figure 24. Differentiation with respect to time yields the penetration velocity

80-4-29

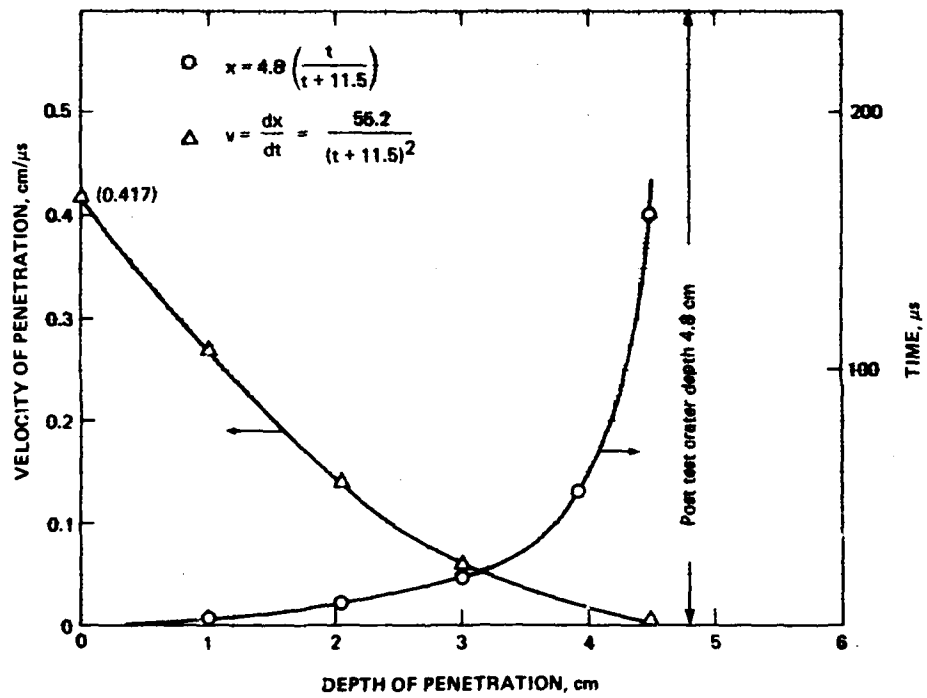


Figure 24 Trajectory and velocity of penetration in aluminum target by Standard Model 4 (LS-3).

$$v_p = \frac{dx}{dt} = \frac{p}{\tau} \left[ \frac{\left(1 + \frac{t}{\tau}\right) - \frac{t}{\tau}}{\left(1 + \frac{t}{\tau}\right)^2} \right]$$

which is also given in Figure 24 for  $p = 4.8$  cm and  $\tau = 11.5$   $\mu$ s. At  $t = 0$ , this gives a penetration velocity of 0.42 cm/ $\mu$ s at the face of the aluminum target.

### 3.5 TARGET DAMAGE

Table 2 summarizes the condition of the aluminum targets that were placed at the end of the models. Here, the models and targets are grouped either by technical objective or by the experimental parameter under investigation. General observations are given in the following subsections.

**3.5.1 Reproducibility of Standard Models.** All of the Standard Models produced deep craters in the aluminum targets. The crater depths ranged from a low of 4.4 cm (Model 1) to a high of 6.3 cm (Model 3), with a mean value of 5.43 cm and a standard deviation of 1.68 cm. The extremes in depth also correspond to the extremes in crater volume, 13 cm<sup>3</sup> and 33 cm<sup>3</sup>. The mean volume was 23.25 cm<sup>3</sup>, with a standard deviation of 14.31 cm<sup>3</sup>.

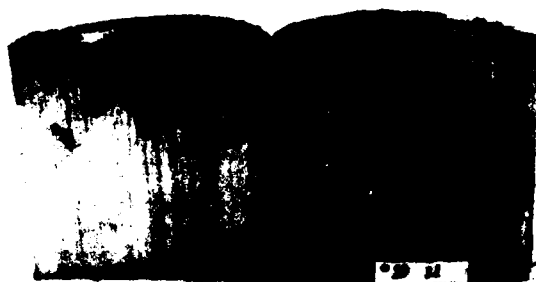
Photographs of the target damage from Standard Models 1, 2, 3, and 4 are given in Figures 25 and 26. These figures show that the shapes of the craters varied considerably. The crater from Model 1 gave evidence of either a spiraling jet or a double jet. Models 2 and 3 had craters that appeared to veer off axis. The cross section of the crater from Model 4 was annular. The diameters of all craters increased with crater depth; Models 1, 2, and 4 increased from 2.0 cm to 2.5 cm, and Model 3 increased 2.7 cm to 3.0 cm.

Table 2 Damage resulting from the various models used in experiment LS-3.

PURPOSE OR POSITION	MODEL POSITION	MODEL TYPE (3/4-inch o.d. 321 stainless steel tubes)	TARGET OR PARAMETER	
			PENETRATION (cm)	SOLE VOLUME (cm <sup>3</sup> )
LOS MODELS (0.012-inch wall, internal pressure <1.0 mm Hg.)				
Reproducibility of Standard	1	Standard No. 1	4.4	13.0
	10	Standard No. 2	6.2	25.0
	11	Standard No. 3	6.3	33.0
	14	Standard No. 4 (without pins)	4.8	22.0
		Average	5.4	23.3
Reproducibility of Polyolefin Spiral	7	Poly Spiral No. 1	--	Pitted Surface --
	8	Poly Spiral No. 2	--	Pitted Surface --
	17	Poly Spiral No. 3	--	Pitted Surface --
Effect of Materials	6	Steel Spiral	--	Pitted Surface --
	5	Lead Spiral	--	Relatively Smooth --
Effect of Geometry	13	Poly Strip	6.3	11.4
Effect of Baffle	12	Thick Lead Spiral Last 12 inches (baffle)	--	Less pitted than poly or steel --
Source Resolution	2	Standard with 4-inch Standoff	5.3	15.5
	3	Standard with 8-inch Standoff	4.9	11.5
	4	Standard with 12-inch Standoff	2.7	8.4
	15	Poly Spiral with 6-inch Spiral	3.9	12.2
	16	Poly Spiral with 9-inch Spiral	1.2	2.8
PINEX MODELS, (0.028-inch wall, internal pressure one atmosphere air)				
Simulation of Pinex Pipe	20	Standard	14.9	61.5
	10	Poly Spiral	--	Pitted Surface --



**STANDARD MODEL #1**



**STANDARD MODEL #2**



**STANDARD MODEL #3**



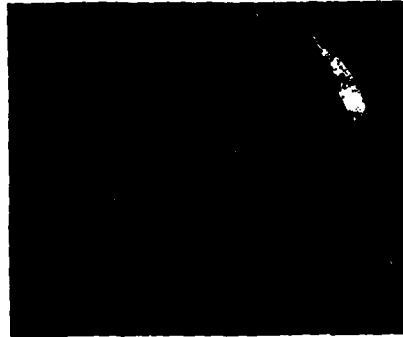
**STANDARD MODEL #4**

80-4-34

**Figure 25** Cross sections of craters produced in aluminum targets by the Standard Models in Experiment LS-3.



**STANDARD MODEL #1**



**STANDARD MODEL #2**



**STANDARD MODEL #3**



**STANDARD MODEL #4**

80-4-35

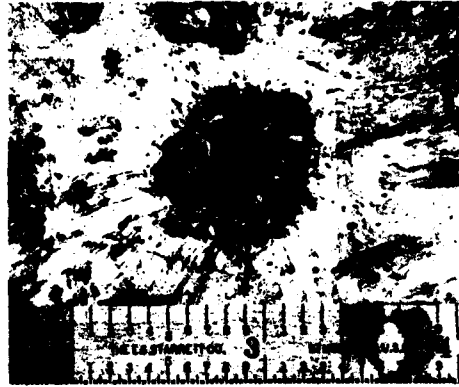
**Figure 26** Surface of the aluminum targets from the Standard Models in Experiment LS-3.

3.5.2 Reproducibility of Polyolefin Spirals. There was considerably less damage to the targets from the Polyolefin Spiral Models (1, 2, and 3). There were no large craters in the targets, but the surfaces of the targets were uniformly pitted with small craters over an area approximately equal to the internal cross-sectional area of the models. The majority of the small craters (pits) had depths which were typically in the range of 0.5 to 1.5 mm. However, each target seemed to have a single small crater with a depth much greater than all of the other craters. These depths were 2.5 mm, 4.6 mm, and 2.0 mm respectively for Models 1, 2, and 3. Photographs of the front surfaces of the targets for these models are given in Figure 27.

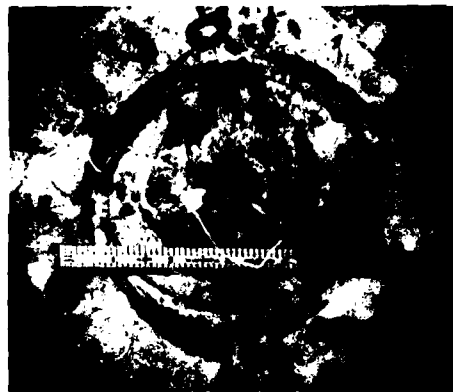
3.5.3 Effect of Materials. The target for the Steel Spiral Model was pitted in a manner similar to those of the Polyolefin Spiral Models, whereas the target for the Lead Model showed less damage. The latter was comparatively smoother. Photographs of these two models are shown in Figure 28.

3.5.4 Effect of Geometry. Unlike the polyolefin spirals, the polyolefin ribbon on the inside surface of this Poly Strip Model produced a crater similar to those from the Standard Models. However, a small hole on one side of the crater produced a crater volume-to-crater depth ratio in this target that was much smaller than the Standard Models. Figure 29 provides a photograph of the target from this model.

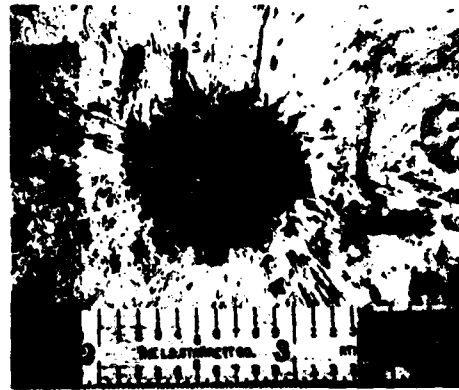
3.5.5 Effect of Baffle. The thick lead baffle is located in the last 24 inches (61 cm) of the model, and conceptually suppresses the jet after it is well formed. This Baffle Model also produced small craters in the target (Figure 30) comparable to those in the Lead Spiral Model.



POLY SPIRAL MODEL #1



POLY SPIRAL MODEL #2



POLY SPIRAL MODEL #3

80-4-36

Figure 27 Surface of the aluminum targets from the Poly Spiral Models in Experiment LS-3.



**STEEL SPIRAL MODEL**



**STEEL SPIRAL MODEL (Close-up View)**



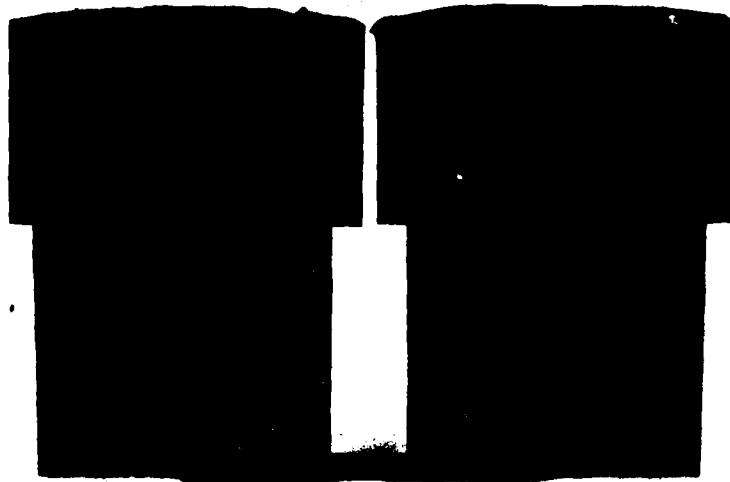
**LEAD SPIRAL MODEL**



**LEAD SPIRAL MODEL (Close-up View)**

80-4-37

**Figure 28** Surface of the aluminum targets from the Steel and Lead Spiral Models in Experiment LS-3.



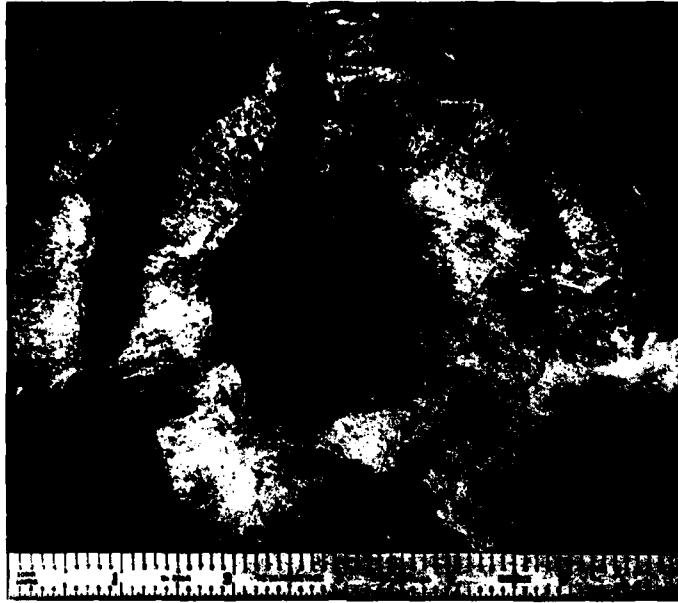
**CROSS SECTION**



**SURFACE**

80-4-38

**Figure 29** Cross section and front surface of the aluminum target from the Poly Strip Model in Experiment LS-3.



80-4-39

**CLOSE-UP VIEW**

**Figure 30** Surface of the aluminum target from the Lead Baffle Model in Experiment LS-3.

3.5.6 Source Resolution. Two types of models are included in this grouping, the Standard Models with Standoffs and the Polyolefin Spiral Models with short spirals near the explosive end of the model. Figures 31 and 32 show photographs of the targets for the Standard Models with standoff. The Polyolefin Spiral Models with short spirals are shown in Figures 33 and 34.

The depths of target penetration for these models are plotted in Figure 35 as a function of the relevant length of standoff or spiral length. The extrapolated values for zero penetration should be the length required for no target damage, i.e., a spiral length of 24.5 cm or a standoff distance of 33.0 cm. Figure 36 is a similar presentation using the crater volume in the target. Here the spiral length required for no crater volume is 25.0 cm, a value in excellent agreement with the depth data. However, there does not appear to be a similar correlation with the standoff distance.

3.5.7 Simulation of Pinex Pipe. As shown in the photographs provided in Figures 37 and 38, the Pinex-Standard Model and Pinex-Polyolefin Spiral Model produced the most dramatic difference in target damage. The Standard Model (Figure 37) produced a crater with a depth of 14.9 cm and a volume of  $61.5 \text{ cm}^3$ . These values were factors of 2.75 and 2.64 higher, respectively, than the corresponding average values from the LOS Standard Models. At the other extreme, the Pinex-Polyolefin Spiral Model merely pitted the surface of the target in a manner similar to the LOS Poly Spiral Models.



**STANDARD MODEL WITH  
4-IN. (10.2 cm) STANDOFF**



**STANDARD MODEL WITH  
8-IN. (20.3 cm) STANDOFF**



**STANDARD MODEL WITH  
12-IN. (30.5 cm) STANDOFF**

80-4-40

**Figure 31** Cross sections of craters produced in the aluminum targets by the Standard Models with Standoffs in Experiment LS-3.



**STANDARD MODEL WITH  
4-IN. (10.2 cm) STANDOFF**



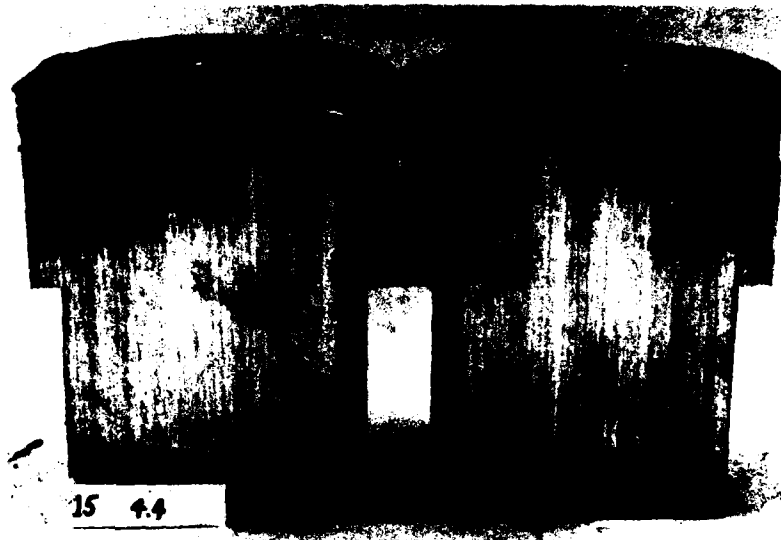
**STANDARD MODEL WITH  
8-IN. (20.3 cm) STANDOFF**



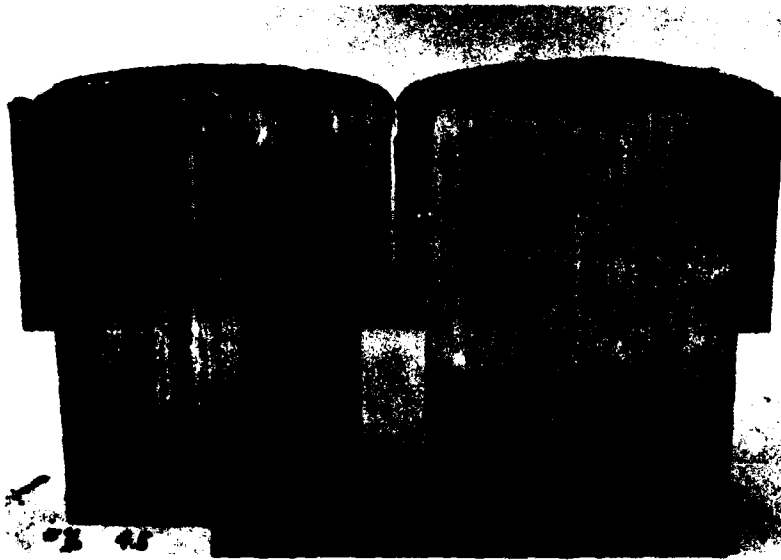
**STANDOFF MODEL WITH  
12-IN. (30.5 cm) STANDOFF**

80-4-41

**Figure 32 Surface of aluminum targets from the Standard Models with Standoffs in Experiment LS-3.**

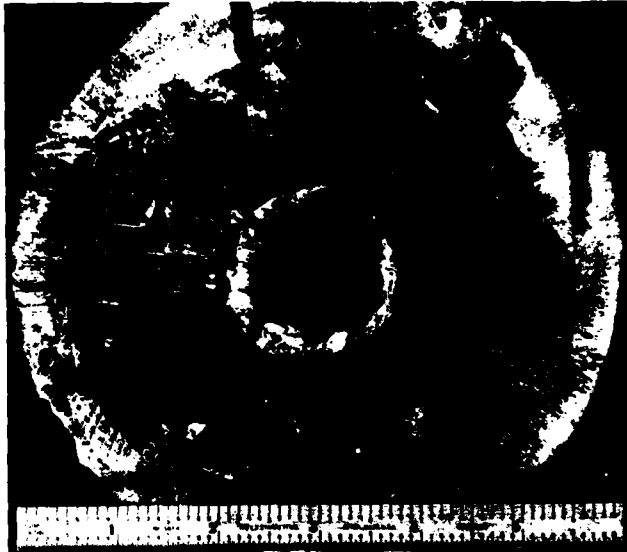


**POLY SPIRAL MODEL WITH  
6-IN. (15.2 cm) SPIRAL**

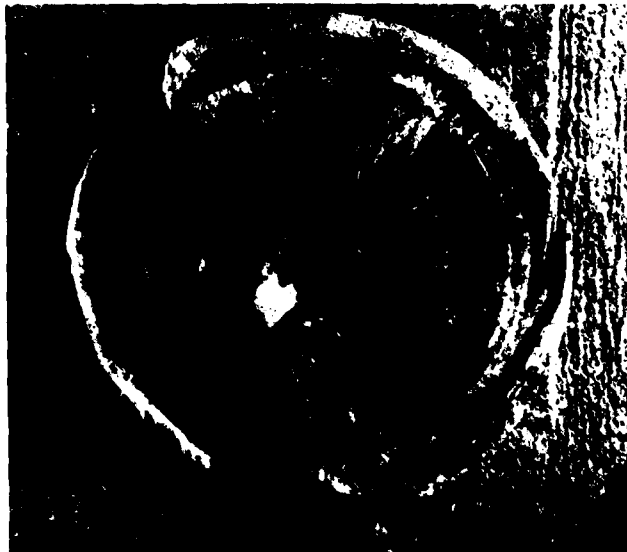


**POLY SPIRAL MODEL WITH  
9-IN. (22.9 cm) SPIRAL**

**Figure 33** Cross sections of craters produced in aluminum targets by the Poly Spiral Models with Short Spirals in Experiment LS-3.



**POLY SPIRAL MODELS WITH  
6-IN. (15.2 cm) SPIRAL**



**POLY SPIRAL MODEL WITH  
9-IN. (22.9 cm) SPIRAL**

80-4-43

**Figure 34** Surface of aluminum targets from the Poly Spiral Models with Short Spirals in Experiment LS-3.

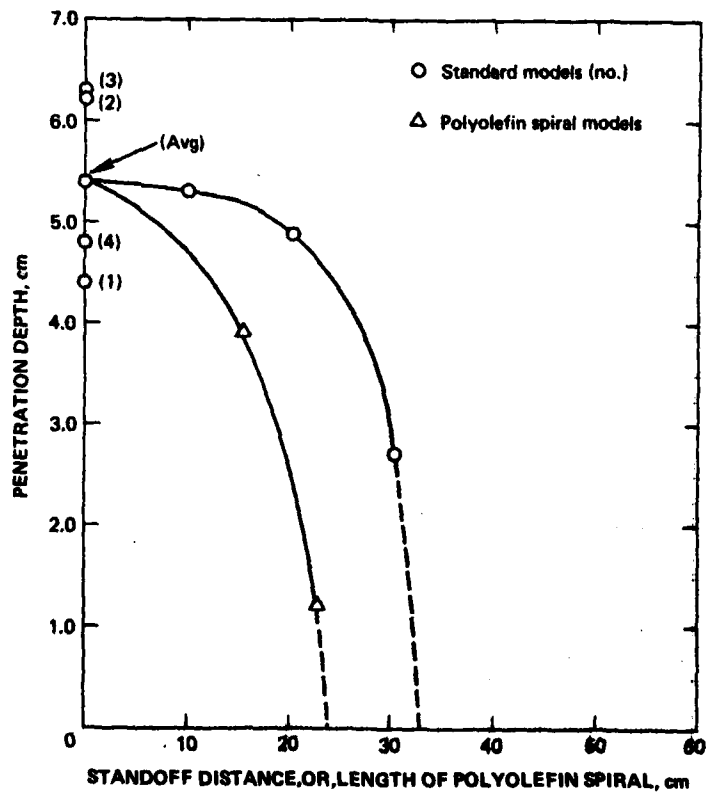
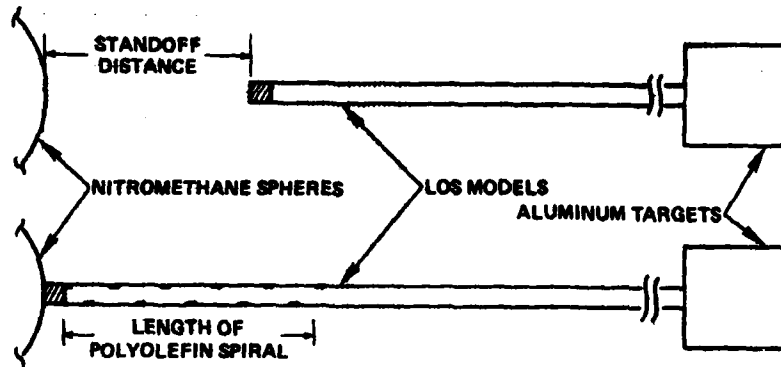
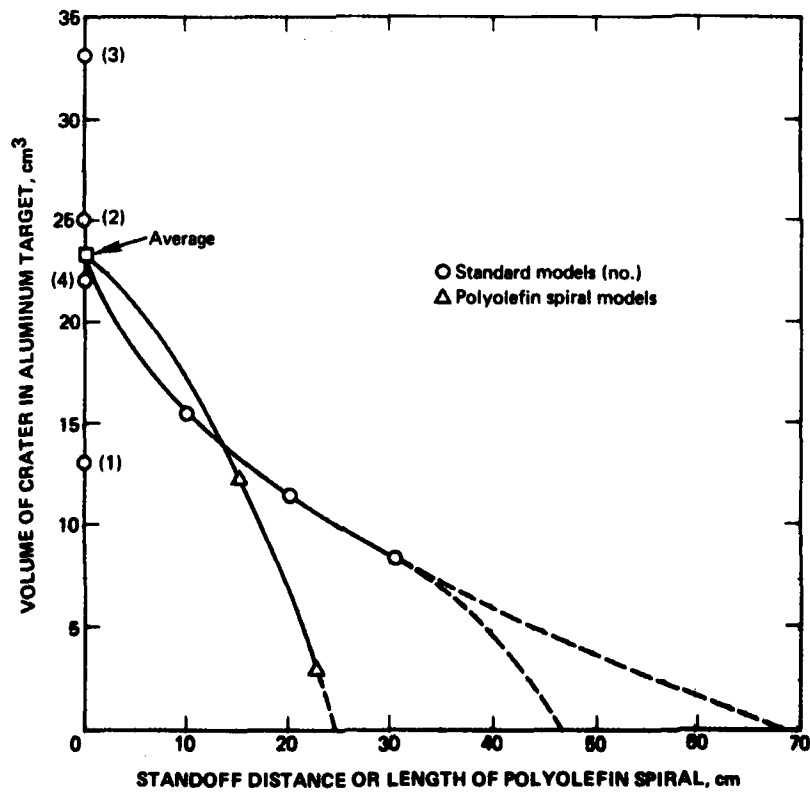
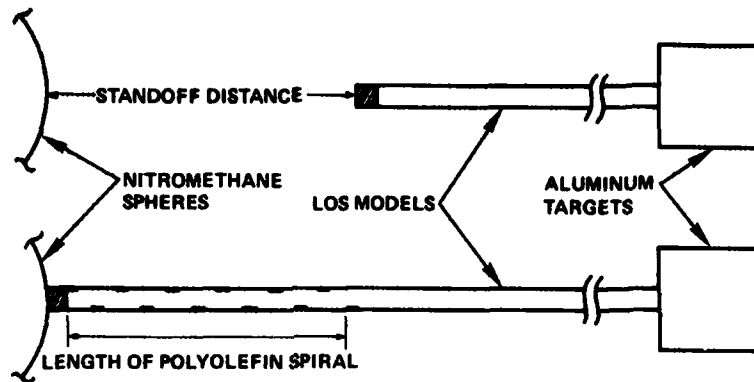


Figure 35 Penetration produced in aluminum targets by LOS models with various lengths of polyolefin spiral and standoff distances.

80-4-30

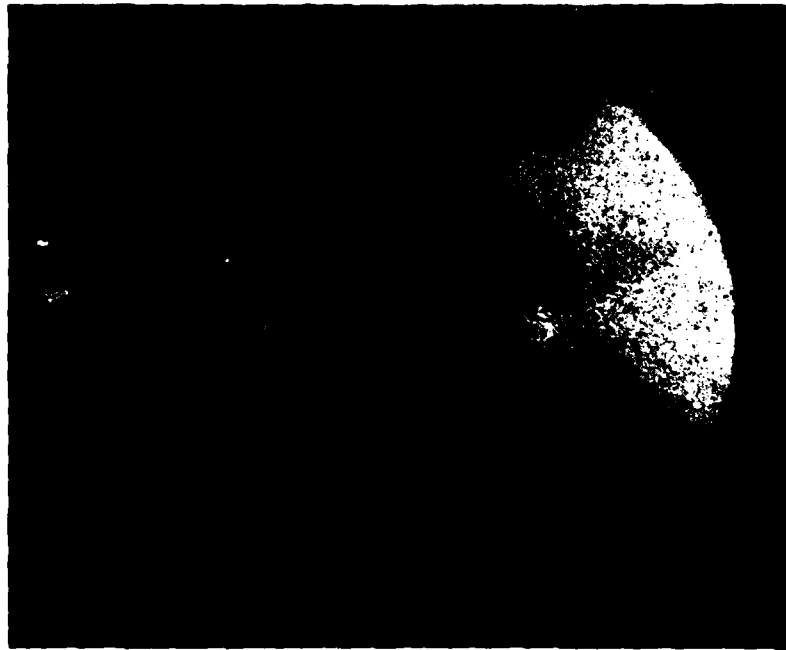


80-4-31

Figure 38 Volume of crater produced in aluminum targets by LOS models with various lengths of polyolefin spiral and standoff distances.



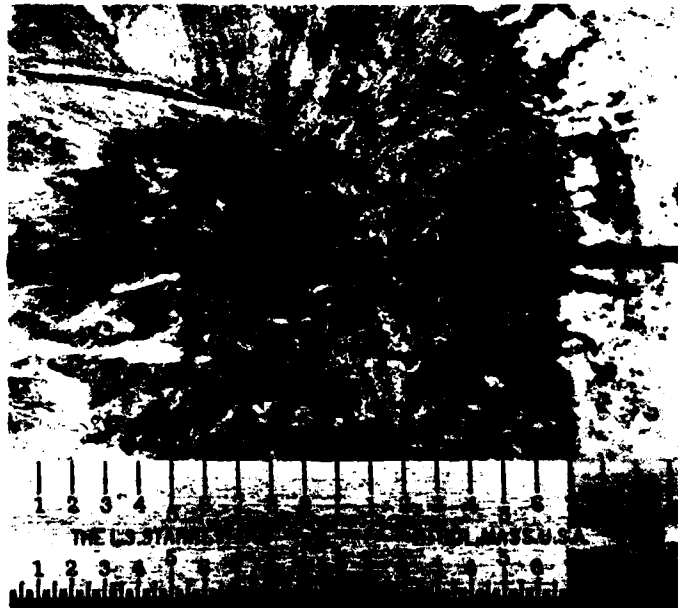
**CROSS SECTION**



**FRONT SURFACE**

**Figure 37** Cross section and front surface of the aluminum target from the Pinex Standard Model in Experiment LS-3.

80-4-44



80-445

CLOSE-UP VIEW

Figure 38 Surface of the aluminum target from the Pinex Model with Poly Spiral in Experiment LS-3.

### 3.6 SUMMARY OF RESULTS

The major findings of this experiment were as follow:

- All of the standard models produced high-energy jets. The jets produced deep craters in aluminum targets located at the end of the models. The target damage from the four identical standard models was not very reproducible. The mean crater depth was 5.4 cm, with a standard deviation of 1.7 cm. The mean crater volume was  $23.3 \text{ cm}^3$ , and had a standard deviation of  $14.3 \text{ cm}^3$ .
- All models with helical asymmetries eliminated high-energy jetting. However, the surfaces of the aluminum targets located at the end of these models were pitted with very small craters. The target damage from three identical models with helical asymmetries was quite reproducible.
- The material used for a helical asymmetry appears to be a relatively unimportant parameter. High-energy jets were eliminated with polyolefin, steel, and lead helixes. While the target conditions from the three different materials were quite comparable, lead produced the least damage and steel produced the most damage to the surface of the target.
- The geometry of an asymmetry appears to be an important parameter. Unlike its helical counterpart, a polyolefin ribbon located on the inside surface of a model, but parallel to the model axis, produced a high-energy jet.

- A thick helical asymmetry, representing a baffle, was located beyond the collapse region of a LOS model, and produced the same results as a thin asymmetry located along the entire length of the model; high-energy jetting was eliminated and target damage was limited to very small craters on the surface of the target.
  
- Based on the depth and volume of craters produced in aluminum targets, a length of polyolefin helix located within the collapse region of a LOS model is more effective in reducing jet energy than removing the same length of model from the collapse process. These data indicate that jetting could be eliminated by a 25-cm length of polyolefin spiral, even though a much longer length of the model contributes to the jet formation. However, it should be noted that such dichotomous results may be due to the poor reproducibility of target damage from high-energy jets.
  
- The jet from a model used to simulate the collapse of a Pinex pipe was found to be more energetic than the jets from the models that were used to simulate a LOS pipe. Still, the jet was eliminated in a Pinex model with a helical ribbon of polyolefin on the inside surface of the model.

In addition to the findings given above, other important results were obtained from the penetration instrumentation that was included on the aluminum target of one of the standard models (No. 4). The data from this instrumentation provided the depth and velocity of the jet as it penetrated the target. The maximum depth of penetration was in good agreement with the post-test

measurement. These data also showed that target penetration is initiated by jetted material which arrives at the target face with a velocity of approximately  $0.6 \text{ cm}/\mu$ . This will have a significant impact on future modeling of the jetting process in LOS models since penetration was previously believed to be initiated by the much faster material ( $\sim 1 \text{ cm}/\mu\text{s}$ ) that first arrives at the aluminum target.

## DISTRIBUTION LIST

### DEPARTMENT OF DEFENSE

Defense Nuclear Agency  
ATTN: SPTD, T. Kennedy  
4 cy ATTN: TITL

Defense Technical Information Center  
12 cy ATTN: DD

Field Command  
Defense Nuclear Agency  
ATTN: FCTMD, W. Summa  
ATTN: FCTK, C. Keller

Field Command Test Directorate  
Test Constructions Division  
Defense Nuclear Agency  
ATTN: FCTC, J. Lacombe

### DEPARTMENT OF ENERGY CONTRACTORS

Nevada Operations Center  
ATTN: R. Newman

Lawrence Livermore National Laboratory  
ATTN: D. Oakley  
ATTN: B. Hudson  
ATTN: B. Terhune  
ATTN: J. Shearer

Los Alamos National Scientific Laboratory  
ATTN: R. Brownlee  
ATTN: E. Jones/F. App  
ATTN: A. Davis  
ATTN: L. Germain  
ATTN: S. Schmidt

Sandia National Laboratories  
Livermore Laboratory  
ATTN: R. Bass  
ATTN: (Div 1111), C. Meh1/C. Smith

### OTHER GOVERNMENT AGENCIES

Department of the Interior  
U.S. Geological Survey  
ATTN: R. Carroll

### DEPARTMENT OF DEFENSE CONTRACTORS

California Research & Technology, Inc  
ATTN: M. Rosenblatt

Pacifica Technology  
ATTN: G. Kent

Physics International  
ATTN: E. Moore

SRI International  
ATTN: A. Florence

Systems, Science & Software  
ATTN: R. Duff

Terra Tek, Inc  
ATTN: S. Green

R & D Associates  
ATTN: P. Haas

General Electric Company—TEMPO  
ATTN: DASIAC

**DATA  
FILM**